Received: 24 April 2020 | Revised: 17 December 2020 | Accepted: 18 January 2021

DOI: 10.1002/rnc.5431

RESEARCH ARTICLE

WILEY

Finite horizon robust synthesis using integral quadratic constraints

Jyot Buch[1] | **Peter Seiler**[2]

[1]Department of Aerospace Engineering and Mechanics, University of Minnesota, 107 Akerman Hall, 110 Union St SE Minneapolis, Minnesota, 55455, USA

[2]Department of Electrical Engineering and Computer Science, University of Michigan, 1301 Beal Ave Ann Arbor, Michigan, 48109, USA

Correspondence
Jyot Buch, Department of Aerospace Engineering and Mechanics, University of Minnesota, Minneapolis, MN 55455.
Email: buch0271@umn.edu

Funding information
Office of Naval Research, Grant/Award Number: N00014-18-1-2209

Abstract

We present a robust synthesis algorithm for uncertain linear time-varying (LTV) systems on finite horizons. The uncertain system is described as an interconnection of a known LTV system and a perturbation. The input–output behavior of the perturbation is specified by time-domain Integral Quadratic Constraints (IQCs). The objective is to synthesize a controller to minimize the worst-case performance. This leads to a nonconvex optimization. The proposed approach alternates between an LTV synthesis step and an IQC analysis step. Both induced $\mathcal{L}_2$ and terminal Euclidean norm penalties on output are considered for finite horizon performance. The proposed algorithm ensures that the robust performance is nonincreasing at each iteration step. The effectiveness of this method is demonstrated using numerical examples.

KEYWORDS

integral quadratic constraints, linear time-varying systems, robust control

1 | INTRODUCTION

This paper considers robust synthesis for uncertain linear time-varying (LTV) systems on finite horizons. This problem is motivated by engineering systems that follow a finite-time trajectory and for which model uncertainty is a significant factor. Examples of such systems include: aircraft landings,[1] missile interceptors,[2] and space-launch or reentry systems.[3-5] The Jacobian linearization of the nonlinear dynamics along the trajectory yields an uncertain, finite horizon LTV system. Robust synthesis can be used to ensure the stability and robustness of the linearized closed-loop over a range of parametric and dynamic uncertainties. Many existing robust synthesis algorithms, for example, μ-synthesis[6-9] have been developed for uncertain linear time-invariant (LTI) system and infinite horizon robustness metrics. This enables the use of frequency-domain techniques. In contrast, this paper is developed for uncertain finite horizon, LTV systems using time-domain techniques.

The specific formulation uses an uncertain system described by an interconnection of a known LTV system and a perturbation. The input–output behavior of the perturbation is described by time-domain Integral Quadratic Constraints (IQCs). The performance objective is specified by an induced gain from $\mathcal{L}_2$ input disturbances to a mixture of an $\mathcal{L}_2$ and terminal Euclidean norm on the output. The objective is to synthesize a controller to minimize the worst-case performance over all allowable uncertainties. This worst-case performance can be used to robustly bound the state at the end of a finite horizon in the presence of external disturbances and model uncertainty.

This robust synthesis problem leads, in general, to a nonconvex optimization. The proposed algorithm, presented in Section 4, iterates between a nominal synthesis step and robustness analysis step. The nominal synthesis step relies on existing finite horizon H_∞ synthesis results which consider a control theoretic formulation.[1,10-12] An alternative game

theoretic formulation is considered in Reference 13 which provides equivalent synthesis conditions. These conditions can be stated in terms of two coupled Riccati Differential Equations (RDEs)[14-16] or two coupled Riccati Differential Inequalities (RDIs).[17] We use the two coupled RDEs as it provides numerical advantage over the RDI conditions. Moreover, in contrast to other work, the results in References 14-16 allow for terminal Euclidean norm penalties on the output. The robustness analysis step uses the IQC framework introduced in References 18,19. This framework has been extended in Reference 20 to assess robustness of the uncertain LTV systems on finite horizons. The approach presented in Reference 20 will be used in this paper for the robustness analysis. Finally, a scaled plant construction is required to link the nominal synthesis and robustness analysis steps.

The proposed method is analogous to the existing DK iteration method for uncertain LTI systems on infinite horizons. The algorithm in this paper generalizes this method to uncertain LTV systems on finite horizons. Similar extensions have been made in References 21,22 for Linear Parameter-Varying (LPV) systems. Two other closely related works are References 23 and 24. The work in Reference 23 considers an extension of the Glover–McFarlane loop-shaping method to LTV systems on infinite horizons. This leads to a robust stabilization problem with a single full block uncertainty. The work in Reference 24 provides convex synthesis conditions for robust performance of uncertain LTV systems. However, Reference 24 assumes that uncertainty lies in a contractive subset and is block partitioned with (2, 2) block being zero. This special structure is used to convexify the synthesis optimization. The algorithm proposed in this paper considers more general robust performance formulation than in References 23 and 24, which allows us to design output-feedback controllers that robustly bound the reachable set of a finite horizon LTV system. A MATLAB implementation of the proposed algorithm including the numerical examples are available in the LTVTools[25] toolbox.

There are three main contributions of the paper. We propose a new iterative algorithm to synthesize robust output feedback controllers of uncertain LTV systems on finite time horizons. This is a continuation of our preliminary work in Reference 26. The distinctions from Reference 26 are as follows: First, we use the dynamic IQC multipliers for the proposed algorithm, whereas the prior work in Reference 26 used the memoryless IQCs and related classes of uncertainties. Second, we use a time-varying IQC factorization to construct a scaled plant. This step ensures that the worst-case gain at each iteration is monotonically nonincreasing. Finally, this paper provides all details and technical proofs regarding the proposed approach. The effectiveness is demonstrated using a nonlinear robot arm example.

1.1 | Notation

Let $\mathbb{R}^{n\times m}$ and $\mathbb{S}^n$ denote the sets of n-by-m real matrices and n-by-n real, symmetric matrices. The finite horizon $\mathcal{L}_2[0,T]$ norm of a (Lebesgue integrable) signal $v:[0,T]\to\mathbb{R}^n$ is $\|v\|_{2,[0,T]} := \left(\int_0^T v(t)^\top v(t)dt\right)^{1/2}$. If $\|v\|_{2,[0,T]}<\infty$ then $v\in\mathcal{L}_2^n[0,T]$. $\mathbb{RL}_\infty$ is the set of rational functions with real coefficients that are proper and have no poles on the imaginary axis. $\mathbb{RH}_\infty\subset\mathbb{RL}_\infty$ contains functions that are analytic in the closed right-half of the complex plane. An abstract formulation using standard Linear Fractional Transformation (LFT) framework[27,28] is used throughout the paper. The notations $\mathcal{F}_l(G,K)$ and $\mathcal{F}_u(N,\Delta)$ represents lower and upper LFTs, respectively. Finally, $G^\sim$ denotes the adjoint of a dynamical system G as formally defined in section 3.2.4 of Reference 11.

2 | PRELIMINARIES

2.1 | Nominal performance

Consider an LTV system H defined on the horizon $[0,T]$:

$$\dot{x}(t) = A(t)\,x(t) + B(t)\,d(t), \tag{1}$$

$$e(t) = C(t)\,x(t) + D(t)\,d(t), \tag{2}$$

where $x(t)\in\mathbb{R}^{n_x}$ is the state, $d(t)\in\mathbb{R}^{n_d}$ is the disturbance input, and $e(t)\in\mathbb{R}^{n_e}$ is the performance output at time $t\in[0,T]$. The state matrices $A:[0,T]\to\mathbb{R}^{n_x\times n_x}$. $B:[0,T]\to\mathbb{R}^{n_x\times n_d}$, $C:[0,T]\to\mathbb{R}^{n_e\times n_x}$, and $D:[0,T]\to\mathbb{R}^{n_e\times n_d}$ are piecewise-continuous (bounded) real matrix valued functions of time. It is assumed throughout that $T<\infty$. Thus $d\in\mathcal{L}_2[0,T]$ implies x and e are in $\mathcal{L}_2[0,T]$ for any initial condition $x(0)$ (chapter 3 of Reference 11). To simplify further, zero

initial conditions are assumed for states, that is, $x(0)=0$. Explicit time dependence of the state matrices is omitted when it is clear from the context. The performance of H will be assessed in terms of an induced gain with two components. First partition the output as follows:

$$\begin{bmatrix} e_I(t) \\ e_E(t) \end{bmatrix} = \begin{bmatrix} C_I(t) \\ C_E(t) \end{bmatrix} x(t) + \begin{bmatrix} D_I(t) \\ 0 \end{bmatrix} d(t), \tag{3}$$

where $e_I(t) \in \mathbb{R}^{n_I}$ and $e_E(t) \in \mathbb{R}^{n_E}$ with $n_e = n_E + n_I$. The generalized performance metric of H is then defined as,

$$\|H\|_{[0,T]} := \sup_{\substack{0 \neq d \in \mathcal{L}_2[0,T] \\ x(0)=0}} \left[\frac{\|e_E(T)\|_2^2 + \|e_I\|_{2,[0,T]}^2}{\|d\|_{2,[0,T]}^2} \right]^{1/2}, \tag{4}$$

This defines an induced gain from the input d to a mixture of an $\mathcal{L}_2$ and terminal Euclidean norm on the output e. This is a useful generalization, as many control design requirements often involve bounding the outputs at final time in addition to bounded control effort. The example discussed in Section 5.2 uses such mixed penalties. More general quadratic cost as in Reference 20 can also be considered with appropriate choice of the input–output matrices (see Appendix A). Note that if $n_E = 0$ then there is no terminal Euclidean norm penalty on the output. This case corresponds to the standard, finite horizon induced $\mathcal{L}_2$ gain of H. Similarly, if $n_I = 0$ then there is no $\mathcal{L}_2$ penalty on the output. This case corresponds to a finite horizon $\mathcal{L}_2$-to-Euclidean gain. This can be used to bound the terminal output $e_E(T)$ resulting from an $\mathcal{L}_2$ disturbance input. Zero feed-through from d to e_E ensures that the Euclidean penalty is well-defined at time $t = T$. The next theorem states an equivalence between a bound on this performance metric $\|H\|_{[0,T]}$ and the existence of a solution to a related RDE (theorem 3.7.4 of Reference 11).

Theorem 1. *Consider an LTV system (1) with $\gamma > 0$ given. Let $Q : [0,T] \to \mathbb{S}^{n_x}$, $S : [0,T] \to \mathbb{R}^{n_x \times n_d}$, $R : [0,T] \to \mathbb{S}^{n_d}$, and $F \in \mathbb{R}^{n_x \times n_x}$ be defined as follows*[*].

$$Q := C_I^\top C_I, \quad S := C_I^\top D_I, \quad R := D_I^\top D_I - \gamma^2 I_{n_d}, \quad F := C_E(T)^\top C_E(T).$$

The following statements are equivalent:

1. $\|H\|_{[0,T]} < \gamma$
2. $R(t) \prec 0$ *for all* $t \in [0,T]$. *Moreover, there exists a differentiable function* $P : [0,T] \to \mathbb{S}^{n_x}$ *such that* $P(T) = F$ *and*

$$\dot{P} + A^\top P + PA + Q - (PB + S)R^{-1}(PB + S)^\top = 0.$$

This is a RDE.

The nominal performance $\|H\|_{[0,T]} < \gamma$ is achieved if the associated RDE solution exists on $[0,T]$ when integrated backward from $P(T) = F$. The assumption $R(t) \prec 0$ ensures $R(t)$ is invertible and hence the RDE is well-defined $\forall t \in [0,T]$. Thus, the solution of the RDE exists on $[0,T]$ unless it grows unbounded. The smallest bound on γ is obtained using bisection.

2.2 | Nominal synthesis

This subsection provides conditions to synthesize a controller that is optimal with respect to the nominal performance metric introduced in the previous subsection. Consider the feedback interconnection shown in Figure 1.

The LTV system G defined on $[0,T]$ is given by:

$$\left[\begin{array}{c} \dot{x}(t) \\ \hline e_I(t) \\ e_E(t) \\ y(t) \end{array}\right] = \left[\begin{array}{c|cc} A(t) & B_d(t) & B_u(t) \\ \hline C_I(t) & 0 & D_{Iu}(t) \\ C_E(t) & 0 & 0 \\ C_y(t) & D_{yd}(t) & 0 \end{array}\right] \left[\begin{array}{c} x(t) \\ \hline d(t) \\ u(t) \end{array}\right], \tag{5}$$

[*] If $n_I = 0$ then $Q = 0_{n_x}$, $S = 0_{n_x \times n_d}$, and $R = -\gamma^2 I_{n_d}$. Similarly, if $n_E = 0$ then $F = 0_{n_x}$.

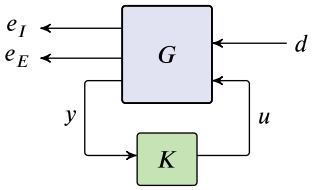

FIGURE 1 Nominal feedback interconnection $\mathcal{F}_l(G,K)$ [Colour figure can be viewed at wileyonlinelibrary.com]

where $d(t) \in \mathbb{R}^{n_d}$ is the generalized disturbance, $u(t) \in \mathbb{R}^{n_u}$ is the control input, and $y(t) \in \mathbb{R}^{n_y}$ is the measured output. The generalized disturbance is of the form $d(t) = \begin{bmatrix} d_{in}(t) \\ n(t) \end{bmatrix}$, where $n(t) \in \mathbb{R}^{n_y}$ is a measurement noise and $d_{in}(t)$ represents all other disturbance inputs. This plant structure also assumes no feedthrough from d to e_E. This is required to ensure that the nominal performance metric is well-posed. In addition, the standard H_∞ synthesis framework imposes additional structure on the matrices relating d to e_I and d to y. This is done to simplify notation and is obtained via standard loop transformations under some minor technical assumptions (chapter 17 of Reference 27). This leads to the following additional structure on the plant matrices:

$$C_I := \begin{bmatrix} 0 \\ C_1 \end{bmatrix} \quad D_{Iu} := \begin{bmatrix} I_{n_u} \\ 0 \end{bmatrix} \quad D_{yd} := \begin{bmatrix} 0 & I_{n_y}. \end{bmatrix}$$

The nominal synthesis problem is to find a causal LTV controller $K : \mathcal{L}_2^{n_y}[0,T] \to \mathcal{L}_2^{n_u}[0,T]$ that optimizes the closed-loop nominal performance, that is:

$$\inf_K \|\mathcal{F}_l(G,K)\|_{[0,T]}.$$

As noted previously, if $n_E = 0$ then the nominal performance metric is the (finite horizon) induced $\mathcal{L}_2$ gain. In this case, the synthesis problem is equivalent to the existing finite horizon H_∞ problem as considered in References 11,12. The theorem below states the necessary and sufficient conditions for existence of a γ-suboptimal controller for the nominal performance metric (with n_E not necessarily equal to zero). Theorem 2 is a special case of results presented in References 14,16.

Theorem 2. *Consider an LTV system (5) with $\gamma > 0$ given. Let B, $\hat{C}$, $\overline{R}$, and $\hat{R}$ be defined as follows.*

$$B := \begin{bmatrix} B_d & B_u \end{bmatrix}, \quad \overline{R} := \mathrm{diag}\{-\gamma^2 I_{n_d}, I_{n_u}\}, \quad \hat{C} := \begin{bmatrix} C_I^\top & C_y^\top \end{bmatrix}^\top, \quad \hat{R} := \mathrm{diag}\{-\gamma^2 I_{n_I}, I_{n_y}\}.$$

1. *There exists an admissible output feedback controller K such that $\|\mathcal{F}_l(G,K)\|_{[0,T]} < \gamma$ if and only if the following three conditions hold:*

(a) *There exists a differentiable function $X : [0,T] \to \mathbb{S}^{n_x}$ such that $X(T) = C_E(T)^\top C_E(T)$,*

$$\dot{X} + A^\top X + XA - XB\overline{R}^{-1}B^\top X + C_I^\top C_I = 0.$$

(b) *There exists a differentiable function $Y : [0,T] \to \mathbb{S}^{n_x}$ such that $Y(0) = 0$,*

$$-\dot{Y} + AY + YA^\top - Y\hat{C}^\top \hat{R}^{-1}\hat{C}Y + B_d B_d^\top = 0.$$

(b) *$X(t)$ and $Y(t)$ satisfy the following point-wise in time spectral radius condition,*

$$\rho(X(t)Y(t)) < \gamma^2, \quad \forall t \in [0,T]. \tag{6}$$

2. *If the conditions above are satisfied, then the closed loop performance $\|\mathcal{F}_l(G,K)\|_{[0,T]} < \gamma$ is achieved by the following central controller:*

$$\dot{\hat{x}}(t) = A_K(t)\,\hat{x}(t) + B_K(t)\,y(t)$$
$$u(t) = C_K(t)\,\hat{x}(t),$$

FIGURE 2 Uncertain system interconnection $\mathcal{F}_u(N, \Delta)$ [Colour figure can be viewed at wileyonlinelibrary.com]

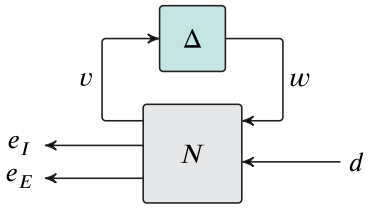

where

$$\begin{aligned} Z &:= (I - \gamma^{-2} YX)^{-1} \\ A_K &:= A + \gamma^{-2} B_d B_d^\top X - ZYC_y^\top C_y - B_u B_u^\top X \\ B_K &:= ZYC_y^\top \\ C_K &:= -B_u^\top X. \end{aligned}$$

For a given $\gamma > 0$, the RDEs associated with X and Y are integrated backward and forward in time, respectively. If solution to both RDEs exist then the spectral radius coupling condition (6) is checked. If all three conditions are satisfied then the central controller achieves a closed-loop performance of γ. The smallest possible value of γ is obtained using bisection. The results in References 14,16 also consider the effect of uncertain initial conditions.

3 | ROBUST PERFORMANCE

3.1 | Uncertain LTV systems

An uncertain, time-varying system $\mathcal{F}_u(N, \Delta)$ is shown in Figure 2. This consists of an interconnection of a known finite horizon LTV system N and a perturbation Δ. This perturbation represents block-structured uncertainties and/or nonlinearities. The term "uncertainty" is used for simplicity when referring to Δ. It is assumed throughout that the interconnection $\mathcal{F}_u(N, \Delta)$ is well-posed. A formal definition for well-posedness is given in References 19,27. The LTV system N is described by the following state-space model:

$$\left[\begin{array}{c} \dot{x}_N(t) \\ \hline v(t) \\ e_I(t) \\ e_E(t) \end{array}\right] = \left[\begin{array}{c|cc} A_N(t) & B_w(t) & B_d(t) \\ \hline C_v(t) & D_{vw}(t) & D_{vd}(t) \\ C_I(t) & D_{Iw}(t) & D_{Id}(t) \\ C_E(t) & 0 & 0 \end{array}\right] \left[\begin{array}{c} x_N(t) \\ \hline w(t) \\ d(t) \end{array}\right]. \tag{7}$$

In addition to notations defined earlier $v \in \mathbb{R}^{n_v}$ and $w \in \mathbb{R}^{n_w}$ are signals associated with the uncertainty Δ. The state vector is denoted as $x_N \in \mathbb{R}^{n_N}$ to refer to the states of system N.

3.2 | Worst-case gain

The robust performance of the uncertain system $\mathcal{F}_u(N, \Delta)$ is assessed using the worst-case gain as defined below.

Definition 1. Let an LTV system N be given by (7) and uncertainty $\Delta : \mathcal{L}_2^{n_v}[0, T] \to \mathcal{L}_2^{n_w}[0, T]$ be in some set $\mathcal{S}$. Assume the interconnection $\mathcal{F}_u(N, \Delta)$ is well-posed. The worst-case gain is then defined as:

$$\gamma_{wc} := \sup_{\Delta \in \mathcal{S}} \|\mathcal{F}_u(N, \Delta)\|_{[0,T]}.$$

The worst-case gain is the largest induced gain of the uncertain time-varying system over all uncertainties Δ in set $\mathcal{S}$. This is difficult to compute directly as it involves an optimization over the entire uncertainty set. Instead, we focus on computing an upper bound on the worst-case gain using dissipation inequalities and IQC conditions.

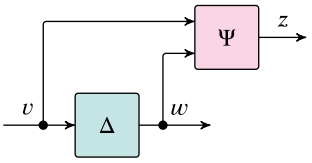

FIGURE 3 Graphical Interpretation for time domain Integral quadratic constraints [Colour figure can be viewed at wileyonlinelibrary.com]

3.3 | Integral quadratic constraints

IQCs[18,19] are used to describe the input–output behavior of Δ. A time-domain formulation is used here for the analysis of the uncertain time-varying system. This formulation is based on the graphical interpretation as shown in Figure 3. Time domain IQCs, as used in this paper, are defined for Δ by specifying a filter Ψ and a finite horizon constraint on the filter output z.

The LTV dynamics of filter Ψ on the horizon $[0, T]$ are given as follows:

$$\begin{bmatrix} \dot{x}_\psi(t) \\ \hline z(t) \end{bmatrix} = \left[\begin{array}{c|cc} A_\psi(t) & B_{\psi v}(t) & B_{\psi w}(t) \\ \hline C_\psi(t) & D_{\psi v}(t) & D_{\psi w}(t) \end{array}\right] \begin{bmatrix} x_\psi(t) \\ \hline v(t) \\ w(t) \end{bmatrix}, \tag{8}$$

where $x_\psi \in \mathbb{R}^{n_\psi}$ is the state. The formal definition for a time-domain IQC is given next.

Definition 2. Consider an LTV system $\Psi : \mathcal{L}_2^{(n_v+n_w)}[0,T] \to \mathcal{L}_2^{n_z}[0,T]$ and $M : [0,T] \to \mathbb{S}^{n_z}$ be given with M piecewise continuous. A bounded, causal operator $\Delta : \mathcal{L}_2^{n_v}[0,T] \to \mathcal{L}_2^{n_w}[0,T]$ satisfies the time domain IQC defined by (Ψ, M) if the following inequality holds for all $v \in \mathcal{L}_2^{n_v}[0,T]$ and $w = \Delta(v)$:

$$\int_0^T z(t)^\top M(t) z(t)\, dt \;\geq 0, \tag{9}$$

where z is the output of Ψ driven by inputs (v, w) with zero initial conditions $x_\psi(0) = 0$.

Note that Definition 2 allows the IQC filter Ψ to be time varying. This time-varying generalization provides an additional degree of freedom for finite horizon robustness analysis with IQCs. Similar generalizations for LPV systems are presented in Reference 29 to use parameter-varying IQCs. However, exploring this additional degree of freedom is a subject of future research. Thus, the examples discussed later in the paper are for the special case where Ψ is an LTI filter. The notation $\Delta \in \mathcal{I}(\Psi, M)$ is used if Δ satisfies the IQC defined by (Ψ, M). A valid IQC $\mathcal{I}(\Psi, M)$ can be defined for a set $\mathcal{S}$ such that $\mathcal{S} \subseteq \mathcal{I}(\Psi, M)$. Two examples are provided below.

Example 1. Let $\mathcal{S}$ denote the set of LTI uncertainties $\Delta \in \mathbb{RH}_\infty$ with $\|\Delta\|_\infty \leq 1$. Let (Ψ, M) be defined as follows:

$$\begin{aligned} \Psi &:= \begin{bmatrix} \Psi_{11} & 0 \\ 0 & \Psi_{11} \end{bmatrix} \text{ with } \Psi \in \mathbb{RH}_\infty^{n_z \times 1} \\ M &:= \begin{bmatrix} M_{11} & 0 \\ 0 & -M_{11} \end{bmatrix} \text{ with } M \in \mathbb{S}^{n_z} \text{ and } M_{11} \succ 0. \end{aligned} \tag{10}$$

It is shown in appendix II of Reference 30 that the pair (Ψ, M) defines a valid time domain IQC for Δ over any $T < \infty$, that is, $\mathcal{S} \subseteq \mathcal{I}(\Psi, M)$.

Example 2. Let $\mathcal{S}$ be the set of LTV parametric uncertainties $\delta(t) \in \mathbb{R}$ with a given norm-bound $\beta(t)$, that is, $w(t) = \delta(t) \cdot v(t)$, $|\delta(t)| \leq \beta(t)$, $\forall t \in [0,T]$. Let $n_v = n_w = n$ and $M_{11} : [0,T] \to \mathbb{S}^n$ be piecewise continuous with $M_{11}(t) \succ 0$, $\forall t \in [0,T]$. Then Δ satisfies the IQC defined by the time-varying matrix:

$$M(t) := \begin{bmatrix} \beta(t)^2\, M_{11}(t) & 0 \\ 0 & -M_{11}(t) \end{bmatrix}, \tag{11}$$

and a static filter $\Psi := I_{2n}$, that is, $\mathcal{S} \subseteq \mathcal{I}(\Psi, M)$.

FIGURE 4 Analysis interconnection [Colour figure can be viewed at wileyonlinelibrary.com]

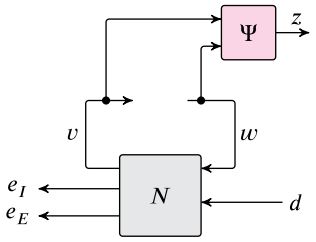

A library of IQCs is provided in References 19,31 for various types of perturbations. Most IQCs are for bounded, causal operators with multipliers Π specified in the frequency domain. Under mild assumptions, a valid time-domain IQC $\mathcal{I}(\Psi, M)$ can be constructed from Π via a J-spectral factorization.[32]

3.4 | Dissipation inequality condition

Consider an extended system as shown in Figure 4. This interconnection includes the IQC filter Ψ but the uncertainty Δ has been removed. The precise relation $w = \Delta(v)$ is replaced, for the analysis, by the constraint on the filter output z.

The extended system of N (Equation (7)) and Ψ (Equation (8)) is governed by the following state space model:

$$\left[\begin{array}{c} \dot{x}(t) \\ \hline z(t) \\ e_I(t) \\ e_E(t) \end{array}\right] = \left[\begin{array}{c|c} \mathcal{A}(t) & \mathcal{B}(t) \\ \hline \mathcal{C}_z(t) & \mathcal{D}_z(t) \\ \mathcal{C}_I(t) & \mathcal{D}_I(t) \\ \mathcal{C}_E(t) & 0 \end{array}\right] \left[\begin{array}{c} x(t) \\ \hline \begin{bmatrix} w(t) \\ d(t) \end{bmatrix} \end{array}\right]. \tag{12}$$

The extended state vector is $x := \begin{bmatrix} x_N \\ x_\psi \end{bmatrix} \in \mathbb{R}^n$ where $n := n_N + n_\psi$. The state-space matrices are given by:

$$\begin{aligned} \mathcal{A} &:= \begin{bmatrix} A_N & 0 \\ B_{\psi v} C_v & A_\psi \end{bmatrix}, \mathcal{B} := \begin{bmatrix} B_w & B_d \\ B_{\psi v} D_{vw} + B_{\psi w} & B_{\psi v} D_{vd} \end{bmatrix} \\ \mathcal{C}_z &:= \begin{bmatrix} D_{\psi v} C_v & C_\psi \end{bmatrix}, \mathcal{C}_I := \begin{bmatrix} C_I & 0 \end{bmatrix}, \mathcal{C}_E := \begin{bmatrix} C_E & 0 \end{bmatrix} \\ \mathcal{D}_z &:= \begin{bmatrix} D_{\psi v} D_{vw} + D_{\psi w} & D_{\psi v} D_{vd} \end{bmatrix}, \mathcal{D}_I = \begin{bmatrix} D_{Iw} & D_{Id} \end{bmatrix}. \end{aligned}$$

The following differential linear matrix inequality (DLMI) is used to compute an upper bound on the worst-case gain of $\mathcal{F}_u(N, \Delta)$.

$$\begin{bmatrix} \dot{P} + \mathcal{A}^\top P + P\mathcal{A} & P\mathcal{B} \\ \mathcal{B}^\top P & 0 \end{bmatrix} + \begin{bmatrix} Q & S \\ S^\top & R \end{bmatrix} + \begin{bmatrix} \mathcal{C}_z^\top \\ \mathcal{D}_z^\top \end{bmatrix} M \begin{bmatrix} \mathcal{C}_z & \mathcal{D}_z \end{bmatrix} \leq -\epsilon I. \tag{13}$$

This inequality depends on the IQC matrix M. It is compactly denoted as $\mathrm{DLMI}_{\mathrm{Rob}}(P, M, \gamma^2, t) \leq -\epsilon I$. This notation emphasizes that the constraint is a DLMI in (P, M, γ^2) for fixed N, Ψ, and (Q, S, R, F). The next theorem states a sufficient DLMI condition to bound the generalized (robust) induced performance measure of $\mathcal{F}_u(N, \Delta)$. The proof is similar to theorem 6 and 7 of Reference 20 and is given below for completeness. It uses IQCs[19] and a standard dissipation argument.[33-35]

Theorem 3. *Consider an LTV system N given by (7) and let* $\Delta : \mathcal{L}_2^{n_v}[0, T] \to \mathcal{L}_2^{n_w}[0, T]$ *be an operator. Assume* $\mathcal{F}_u(N, \Delta)$ *is well-posed and* $\Delta \in \mathcal{I}(\Psi, M)$. *Let* $Q : [0, T] \to \mathbb{S}^n$, $S : [0, T] \to \mathbb{R}^{n \times (n_w + n_d)}$, $R : [0, T] \to \mathbb{S}^{(n_w + n_d)}$, *and* $F \in \mathbb{R}^{n \times n}$ *be defined as follows.*

$$Q := C_I^\top C_I, \quad S := C_I^\top \mathcal{D}_I, \quad R := \mathcal{D}_I^\top \mathcal{D}_I - \gamma^2 \mathrm{diag}\{0_{n_w}, I_{n_d}\}, \quad F := C_E(T)^\top C_E(T). \tag{14}$$

If there exists $\epsilon > 0$, $\gamma > 0$ and a differentiable function $P : [0,T] \to \mathbb{S}^n$ such that $P(T) \geq F$ and,

$$DLMI_{Rob}(P, M, \gamma^2, t) \leq -\epsilon I \qquad \forall t \in [0,T], \tag{15}$$

then $\|\mathcal{F}_u(N,\Delta)\|_{[0,T]} < \gamma$.

Proof. Let $d \in \mathcal{L}_2[0,T]$ and $x_N(0) = 0$ be given. By well-posedness, $F_u(N,\Delta)$ has a unique solution (x_N, v, w, e_I, e_E). Define $x := \begin{bmatrix} x_N \\ x_\psi \end{bmatrix}$. Then (x, z, e_I, e_E) are a solution of the extended system (12) with inputs (w,d) and initial condition $x(0) = 0$. Moreover, z satisfies the the IQC defined by (Ψ, M). Define a storage function by $V(x,t) := x^\top P(t) x$. Left and right multiply the DLMI (13) by $[x^\top, w^\top, d^\top]$ and its transpose to show that V satisfies the following dissipation inequality for all $t \in [0,T]$:

$$\dot{V} + \left[\begin{bmatrix} x \\ \begin{bmatrix} w \\ d \end{bmatrix} \end{bmatrix}^\top \begin{bmatrix} Q & S \\ S^\top & R \end{bmatrix} \left[\begin{bmatrix} x \\ \begin{bmatrix} w \\ d \end{bmatrix} \end{bmatrix} + z^\top M z \leq -\epsilon\ d^\top d. \tag{16}$$

Use the choices for (Q,S,R) to rewrite the second term as $e_I^\top e_I - \gamma^2 d^\top d$. Integrate over $[0,T]$ to obtain:

$$x(T)^\top P(T) x(T) + \int_0^T z(t)^\top M(t) z(t)\ dt + \|e_I\|_{2,[0,T]}^2 \leq (\gamma^2 - \epsilon)\|d\|_{2,[0,T]}^2.$$

Apply $P(T) \geq F = C_E(T)^\top C_E(T)$ and $\Delta \in \mathcal{I}(\Psi, M)$ to conclude:

$$\|e_E(T)\|_2^2 + \|e_I\|_{2,[0,T]}^2 \leq (\gamma^2 - \epsilon)\|d\|_{2,[0,T]}^2. \tag{17}$$

This inequality implies $\|F_u(N,\Delta)\|_{[0,T]} < \gamma$. ∎

3.5 | Computational approach

Numerical implementation using IQCs often involve a fixed choice of Ψ and optimization subject to the convex constraints on M. Two examples are provided as follows.

Example 3. Consider an LTI uncertainty $\Delta \in \mathbb{RH}_\infty$ with $\|\Delta\|_\infty \leq 1$. By Example 1, Δ satisfies any IQC (Ψ, M) with $\Psi := \begin{bmatrix} \Psi_{11} & 0 \\ 0 & \Psi_{11} \end{bmatrix}$, $M := \begin{bmatrix} M_{11} & 0 \\ 0 & -M_{11} \end{bmatrix}$, and $M_{11} \succ 0$. A typical choice for Ψ_{11} is:

$$\Psi_{11} := \left[1, \frac{1}{(s+p)}, \ \dots\ \frac{1}{(s+p)^q}\right]^\top \ \text{with}\ \ p > 0. \tag{18}$$

The analysis is performed by selecting (p,q) to obtain (fixed) Ψ and optimizing over the convex constraint $M_{11} \succ 0$. The results depend on the choice of (p,q). Larger values of q represent a richer class of IQCs and hence yield less-conservative results but with increasing computational cost. Note that the IQC filter Ψ is not square in general with $n_z = 2(q+1)$ outputs.

Example 4. Conic combinations of multiple IQCs can be incorporated in analysis. Let (Ψ_i, M_i) with $i = 1, 2, \dots, N$ define N valid IQCs for Δ. Hence $\int_0^T z_i^\top M_i z_i\ dt \geq 0$ where z_i is the output Ψ_i driven by v and $w = \Delta(v)$. The multiple constraints can be multiplied by $\lambda_i \geq 0$ and combined to yield:

$$\int_0^T \sum_{i=1}^N \lambda_i z_i^\top M_i z_i\ dt \geq 0. \tag{19}$$

FIGURE 5 Uncertain feedback interconnection $\mathcal{F}_u(\mathcal{F}_l(G,K),\Delta)$ [Colour figure can be viewed at wileyonlinelibrary.com]

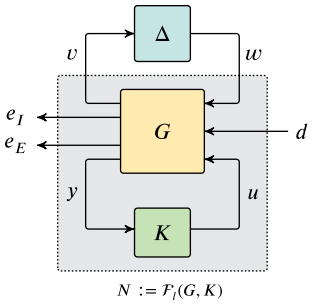

Thus a valid time-domain IQC for Δ is given by

$$\Psi := \begin{bmatrix} \Psi_1 \\ \vdots \\ \Psi_N \end{bmatrix} \text{ and } M(\lambda) := \begin{bmatrix} \lambda_1 M_1 & & \\ & \ddots & \\ & & \lambda_N M_N. \end{bmatrix} \tag{20}$$

The analysis optimizes over λ given selected (Ψ_i, M_i).

An iterative algorithm given in Reference 20 is used in this paper to compute the smallest upper bound on the worst-case gain. It combines the DLMI formulation in the Theorem 3 with a related RDE. The algorithm returns the upper bound $\overline{\gamma}_{wc}$ along with the decision variables P and M.

4 | ROBUST SYNTHESIS

4.1 | Problem formulation

An uncertain feedback interconnection is shown in Figure 5 where G is an LTV system on $[0, T]$ and Δ is assumed to lie in some set S that is described by valid time domain IQCs.

The finite horizon robust synthesis problem is to synthesize a controller which minimizes the impact of both worst-case disturbances and worst-case uncertainties, that is:

$$\inf_K \sup_{\Delta \in S} \|\mathcal{F}_u(\mathcal{F}_l(G,K),\Delta)\|_{[0,T]}. \tag{21}$$

Let the LTV system G defined on $[0, T]$ be given as:

$$\left[\begin{array}{c} \dot{x}_G(t) \\ \hline v(t) \\ e_I(t) \\ e_E(t) \\ y(t) \end{array}\right] = \left[\begin{array}{c|ccc} A_G(t) & B_w(t) & B_d(t) & B_u(t) \\ \hline C_v(t) & D_{vw}(t) & D_{vd}(t) & D_{vu}(t) \\ C_I(t) & D_{Iw}(t) & D_{Id}(t) & D_{Iu}(t) \\ C_E(t) & 0 & 0 & 0 \\ C_y(t) & D_{yw}(t) & D_{yd}(t) & D_{yu}(t) \end{array}\right] \left[\begin{array}{c} x_G(t) \\ \hline w(t) \\ d(t) \\ u(t) \end{array}\right], \tag{22}$$

where $x_G \in \mathbb{R}^{n_G}$ is the state. This plant structure has no feedthrough from d to e_E for well-posedness. The synthesis problem (21) involves the worst-case gain computed over the entire uncertainty set. As noted earlier, instead we focus on minimizing worst-case gain upper bounds. In other words, we define IQCs $\mathcal{I}(\Psi, M)$ such that $S \subseteq \mathcal{I}(\Psi, M)$ and maximize over $\Delta \in \mathcal{I}(\Psi, M)$ in Equation (21). The goal is to design a LTV controller $K : \mathcal{L}_2^{n_y}[0, T] \to \mathcal{L}_2^{n_u}[0, T]$ to minimize the worst-case gain upper bound on $\mathcal{F}_u(\mathcal{F}_l(G,K),\Delta)$. This leads to a nonconvex synthesis problem and involves solving for the controller as well as IQC multipliers.

The approach taken here is to decompose the synthesis into two subproblems. First, solve a nominal synthesis problem (on a specially constructed scaled plant) to obtain K. Second, solve an IQC analysis problem to compute the worst-case gain upper bound. These subproblems can be solved iteratively, similar to coordinate descent, to get a reasonable

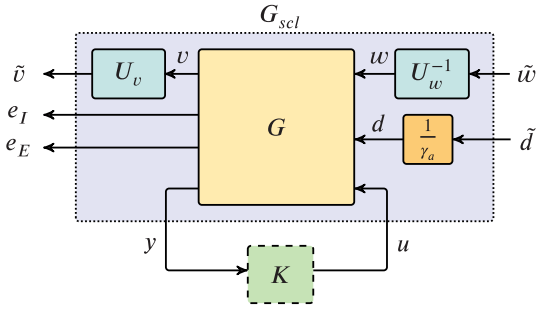

FIGURE 6 Linear time-varying synthesis on scaled plant G_{scl} [Colour figure can be viewed at wileyonlinelibrary.com]

suboptimal solution. The proposed algorithm utilizes this approach to obtain a finite horizon suboptimal controller. As with DK synthesis, there are no guarantees that the coordinate-wise iteration will lead to a local optima let alone a global optima. However, it is a useful heuristic that will enable the robust synthesis to extended naturally from LTI to finite horizon LTV systems. The following assumption is made for the structure of IQC matrix M and filter Ψ.

Assumption 1. The IQC decision variables $M : [0, T] \to \mathbb{S}^{n_z}$ for a specified IQC filter $\Psi : \mathcal{L}_2^{(n_v+n_w)}[0, T] \to \mathcal{L}_2^{n_z}[0, T]$ are assumed to have the following block diagonal structure

$$M(t) := \begin{bmatrix} M_v(t) & 0 \\ 0 & -M_w(t) \end{bmatrix}, \quad \Psi := \begin{bmatrix} \Psi_v & 0 \\ 0 & \Psi_w \end{bmatrix},$$

with constraints $M_v(t) \succ 0$ and $M_w(t) \succ 0$, $\forall t \in [0, T]$. Moreover, Ψ has a feedthrough matrix $D_\psi(t) := \begin{bmatrix} D_{\psi v}(t) & D_{\psi w}(t) \end{bmatrix} \in \mathbb{R}^{n_z \times (n_v+n_w)}$ with full column rank $\forall t \in [0, T]$.

This block diagonal assumption is made to simplify the notation. More general IQC multipliers are considered for (infinite horizon) synthesis in Reference 9. As discussed in Example 3, the IQC filter Ψ, is typically prespecified by a collection of basis functions. In this case, the worst-case gain condition in Theorem 3 is a differential LMI in the variables M_v, M_w, P, and γ^2. The filter Ψ is, in general, nonsquare with $n_z \neq n_v + n_w$. The proposed synthesis method requires a nonunique factorization such that resulting factor is invertible square system, that is, $n_z = n_v + n_w$. The finite horizon factorization (Lemma 2 in Appendix B) can be used to construct square invertible systems U_v and U_w such that,

$$\begin{aligned} \Psi_v^\sim M_v \Psi_v &= U_v^\sim U_v \\ \Psi_w^\sim M_w \Psi_v &= U_w^\sim U_w. \end{aligned} \tag{23}$$

The assumption that feedthrough matrix $D_\psi(t)$ has full column rank is required for the existence of such factorization. This factorization is used in the proposed synthesis algorithm below to construct a scaled plant.

4.2 | Algorithm

A high-level overview of the proposed iterative method is given in Algorithm 1. The uncertain finite horizon system is $\mathcal{F}_u(\mathcal{F}_l(G, K), \Delta)$ with G given by Equation (22) and Δ specified by uncertainty set $\mathcal{I}(\Psi, M)$. The robust synthesis algorithm is specified to run a given maximum number of iterations N_{syn}. It is initialized with scalings $U_v^{(0)} := I_{n_v}$ and $U_w^{(0)} := I_{n_w}$. There is also an initial performance scaling set to $\gamma_a^{(0)} := 1$.

The beginning of each iteration involves the construction of a scaled plant G_{scl} as shown in Figure 6. This step is described further in the next subsection. For now, it is sufficient to note that $G_{\text{scl}} = G$ on the first iteration due to the initialization choices. The next step is to perform finite horizon nominal synthesis on the scaled plant. This step is performed using the synthesis results described previously in Section 2.2. This yields a controller $K^{(i)}$ and the achievable closed-loop performance $\gamma_s^{(i)}$. Each iteration concludes with an IQC analysis on the uncertain closed-loop of $N := \mathcal{F}_l(G, K^{(i)})$ and Δ as shown in Figure 5. This closed-loop uses the original (unscaled) plant G and the controller $K^{(i)}$ obtained from the nominal synthesis step. The worst-case gain upper bound $\gamma_a^{(i)}$ is computed using the algorithm in Reference 20 as summarized in Section 3. This iterative algorithm requires additional initialization including number of analysis iterations N_{iter}, stopping

Algorithm 1. Finite horizon robust synthesis

1: **Given:** G
2: **Initialize:** N_{syn}, $U_v^{(0)} := I_{n_v}$,$U_w^{(0)} := I_{n_w}$, $\gamma_a^{(0)} := 1$
3: **for** $i = 1 : N_{\text{syn}}$ **do**
4: **Scaled Plant Construction (Section 4.3):** Construct a scaled plant $G_{\text{scl}}^{(i)}$ using G, $U_v^{(i-1)}$,$U_w^{(i-1)}$, $\gamma_a^{(i-1)}$.
Output: $G_{\text{scl}}^{(i)}$
5: **Nominal LTV Synthesis (Section 2.2):** Perform nominal controller synthesis on the scaled plant $G_{\text{scl}}^{(i)}$.
Output: $K^{(i)}$, $\gamma_s^{(i)}$
6: **IQC Analysis (Section 3):** Choose the basis functions for Ψ and perform worst-case gain iterations on $\mathcal{F}_u(N^{(i)}, \Delta)$ using iterative algorithm presented in 20 where $N^{(i)} := \mathcal{F}_l(G, K^{(i)})$ denotes the closed loop LTV system. Perform finite horizon factorization using the same Ψ and computed decision variables $M^{(i)}$ to compute the uncertainty channel scalings $U_v^{(i)}$ and $U_w^{(i)}$.
Output: $P^{(i)}$, $M^{(i)}$, $\gamma_a^{(i)}$, $U_v^{(i)}$, $U_w^{(i)}$
7: **end for**

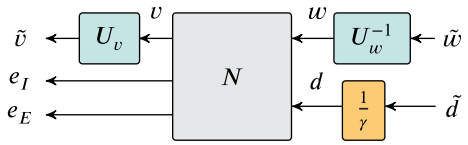

FIGURE 7 Scaled plant N_{scl} [Colour figure can be viewed at wileyonlinelibrary.com]

tolerance *tol*, DLMI time grid t_{DLMI} and spline basis function time grid t_{sp}, which are not included in Algorithm 1. All subsequent iterations require the construction of a scaled plant using the IQC results. The construction of this scaled plant links together the nominal synthesis and IQC analysis steps. It is described further in Section 4.3. Algorithm 1 terminates after N_{syn} iterations. More sophisticated stopping conditions can be employed. For example, the iterations could be terminated if no significant improvement in worst-case gain is achieved. The algorithm returns the controller of order n_K that achieves the best (smallest) bound on the worst-case gain, where $n_K = n_G + n_\psi$.

4.3 | Construction of a scaled plant

The scaled open loop plant $G_{\text{scl}}^{(i)}$ is constructed as shown in Figure 6 by scaling the performance channels and uncertainty channels of original open loop plant G using $U_v^{(i-1)}$, $U_w^{(i-1)}$ and $\gamma_a^{(i-1)}$ obtained from the previous iteration. This scaling ensures appropriate normalization of the performance and uncertainty channels. This is a key step which integrates the nominal synthesis and worst-case gain problem. To simplify the notation, the superscripts $(i-1)$ will be dropped in the remainder of this subsection.

Let $N := \mathcal{F}_l(G, K)$ be the closed-loop (without uncertainty). For a given IQC filter Ψ an extended system N_{ext} similar to Figure 4 can be constructed. The next lemma gives a formal statement connecting robust performance of the extended system N_{ext} to nominal performance of scaled system N_{scl} as shown in Figure 7.

Lemma 1. *Let $\epsilon > 0$, $\gamma > 0$, $M_v(t) \succ 0$, $M_w(t) \succ 0$ and a differentiable function $P : [0, T] \to \mathbb{S}^n$ such that $P(T) \geq F$ be given with the choice of (Q, S, R, F) as in Equation (14). The following statements are equivalent:*

1. $\text{DLMI}_{\text{Rob}}(P, M, \gamma^2, t) \leq -\epsilon I, \quad \forall t \in [0, T]$.
2. $\|N_{\text{scl}}\|_{[0,T]} \leq 1 - \hat{\epsilon}$, *for some* $\hat{\epsilon}$.

Proof. A proof of this lemma is given in Appendix C. It uses a time-varying factorization of (Ψ, M) to construct U_v and U_w. ∎

The above lemma states that extended system given by Equation (12) satisfies the robust performance condition (15) if and only if the scaled system has nominal performance less than 1.

4.4 | Main theorem

The plant $G_{\text{scl}}^{(1)} = G$ for the robust synthesis may include the uncertainty and performance channel design weights as in standard robust control workflow.[27,28] These weights can be static, dynamic, and/or time-varying depending on the requirement. Typically, multiple design iterations are performed to tune these weights and yield an acceptable trade-off between robustness and performance. Note that the first nominal LTV synthesis step in Algorithm 1 may not yield a finite performance $\gamma_s^{(1)}$. For example, if the uncertainty level is too high then the RDEs for nominal synthesis of $G_{\text{scl}}^{(1)} = G$ may not have a solution on $[0, T]$ for any finite $\gamma_s^{(1)}$. However, in this case, finite performance can be achieved by reducing the uncertainty level and restarting the iteration. The main theorem is presented next with a technical assumption that the first nominal synthesis step yields a finite performance.

Theorem 4. *If the first nominal synthesis step yields a finite performance $\gamma_s^{(1)}$ then all the subsequent iterations are well-posed at each step and worst-case gain is non-increasing, that is,*

$$\gamma_a^{(i+1)} \leq \gamma_a^{(i)} \quad \forall i \geq 1.$$

Proof. The first iteration ($i = 1$) is different from the subsequent one. Due to initialization choices $G_{\text{scl}}^{(1)} = G$. The synthesis step is performed with no modifications and yields a controller $K^{(1)}$ that guarantees the closed loop performance of $\gamma_s^{(1)}$. By assumption, we have $\gamma_s^{(1)} < \infty$. The IQC analysis step performed on the closed loop $N^{(1)} := \mathcal{F}_l(G, K^{(1)})$ uncertain plant then achieves a finite horizon worst-case gain upper bound of $\gamma_a^{(1)} < \infty$. Thus, the first iteration is well posed.

All subsequent iterations ($i > 1$) begin with the iteration count update in the for loop. The IQC analysis step from previous iteration shows that there exists $(P^{(i-1)}, M^{(i-1)}, \gamma_a^{(i-1)})$ for a chosen Ψ that satisfies DLMI (13). This implies that the finite horizon factorization exists and multipliers $U_v^{(i-1)}$ and $U_w^{(i-1)}$ can be obtained using Lemma 2 in Appendix B. Using these multipliers and worst-case gain $\gamma_a^{(i-1)}$, scaled plant similar to Figure 7 can be constructed. By Lemma 1, this scaled plant satisfies nominal performance <1. Removing the controller yields the scaled open-loop plant $G_{\text{scl}}^{(i)}$. Thus, the construction of a scaled open-loop plant as shown in Figure 6 is well-defined. The synthesis step performed on $G_{\text{scl}}^{(i)}$ optimizes over all time-varying finite horizon controllers to yield a new controller $K^{(i)}$ that guarantees performance $\gamma_s^{(i)} < 1$. This new controller $K^{(i)}$ yields better nominal performance than the previous controller $K^{(i-1)}$ when used with the unscaled plant G. Thus, the closed loop $N^{(i)} := \mathcal{F}_u(G, K^{(i)})$ must satisfy the nominal performance <1 when using $\gamma_a^{(i-1)}$. Lemma 1 can be used backwards in the next analysis step of $N^{(i)}$. Specifically, the closed loop with unscaled plant G and $K^{(i)}$ satisfies the DLMI analysis condition with $(P^{(i-1)}, M^{(i-1)}, \gamma_a^{(i-1)})$. Further, analysis step on $N^{(i)} := \mathcal{F}_l(G, K^{(i)})$ optimizes over all feasible P and M. This yields a worst-case gain $\gamma_a^{(i)}$ no greater than the previous step $\gamma_a^{(i-1)}$. Thus $\forall i \geq 1$, we have $\gamma_a^{(i+1)} \leq \gamma_a^{(i)}$. ∎

5 | NUMERICAL EXAMPLES

5.1 | LTI example

Consider a first order LTI system G with the following dynamics:

$$\dot{x}(t) = 0.5\, x(t) + u(t) + w(t) + d_{in}(t), \tag{24}$$

$$v(t) = u(t) + d_{in}(t), \tag{25}$$

$$e_I(t) = \begin{bmatrix} x(t) \\ 0.2\, u(t) \end{bmatrix}, \tag{26}$$

$$y(t) = x(t) + 0.01\, n(t), \tag{27}$$

where the performance output is $e_I(t) \in \mathbb{R}^2$ and measurement output is $y(t) \in \mathbb{R}$. The generalized disturbance input is $d(t) := \begin{bmatrix} d_{in}(t) \\ n(t) \end{bmatrix}$ where $d_{in}(t) \in \mathbb{R}$ is an external disturbance input and $n(t) \in \mathbb{R}$ is a measurement noise. Δ is a norm

FIGURE 8 Two-link planar robot[36] [Colour figure can be viewed at wileyonlinelibrary.com]

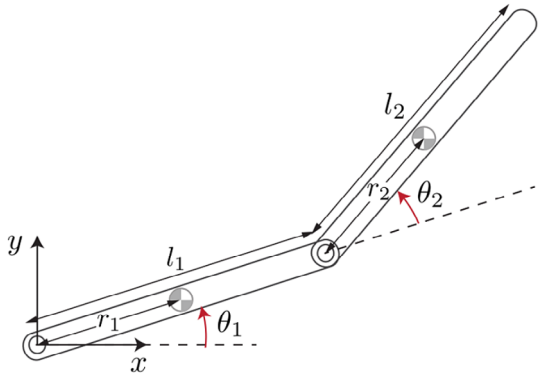

bounded, time-varying, nonlinear uncertainty with norm bound $\beta = 0.6$. The goal is to design a measurement feedback controller K that minimizes the worst-case-induced $\mathcal{L}_2$-gain from disturbance d to output e_I.

First, an infinite horizon robust synthesis is performed to minimize the worst-case gain of the closed loop system. This is achieved by performing bisection on the gain γ for a scaled plant until the robust performance is equal to 1. At each bisection step, MATLAB's `musyn` function is called to optimize the structured singular value upper bound $\overline{\mu}$. This function uses an iterative control design process (DK-iteration) to optimizes the $\overline{\mu}$ of the closed loop system. The infinite horizon worst-case-induced $\mathcal{L}_2$-gain for the designed robust controller is 0.0563. Next, finite horizon robust synthesis is performed on a relatively long horizon (i.e., $T = 300$ s) using the method proposed in this paper. The closed-loop worst-case gain achieved by a finite horizon time-varying controller is computed as 0.0560. This simple comparison results show that on a relatively long horizon the worst-case gain achieved using the finite horizon controller approaches to that of the value achieved by an infinite horizon controller. Note that the proposed method uses purely time-domain approach whereas the μ-synthesis method uses the frequency gridding approach to approximate $\overline{\mu}$ and the associated D-scales. Thus, the close agreement between the two worst-case gains on this example may not hold in general.

5.2 | Nonlinear example

Consider an example of a two-link robot arm as shown in the Figure 8. The mass and moment of inertia of the ith link are denoted by m_i and I_i. The robot properties are $m_1 = 3\,\text{kg}$, $m_2 = 2\,\text{kg}$, $l_1 = l_2 = 0.3\,\text{m}$, $r_1 = r_2 = 0.15\,\text{m}$, $I_1 = 0.09\ \text{kg}\cdot\text{m}^2$, and $I_2 = 0.06\ \text{kg}\cdot\text{m}^2$. The nonlinear equations of motion[36] for the robot are given by:

$$\begin{bmatrix} \alpha + 2\beta\cos(\theta_2) & \delta + \beta\cos(\theta_2) \\ \delta + \beta\cos(\theta_2) & \delta \end{bmatrix} \begin{bmatrix} \ddot{\theta}_1 \\ \ddot{\theta}_2 \end{bmatrix} + \begin{bmatrix} -\beta\sin(\theta_2)\dot{\theta}_2 & -\beta\sin(\theta_2)(\dot{\theta}_1 + \dot{\theta}_2) \\ \beta\sin(\theta_2)\dot{\theta}_1 & 0 \end{bmatrix} \begin{bmatrix} \dot{\theta}_1 \\ \dot{\theta}_2 \end{bmatrix} = \begin{bmatrix} \tau_1 \\ \tau_2 \end{bmatrix}$$

with

$$\alpha := I_1 + I_2 + m_1 r_1^2 + m_2(l_1^2 + r_2^2) = 0.4425\ \text{kg}\cdot\text{m}^2$$
$$\beta := m_2 l_1 r_2 = 0.09\ \text{kg}\cdot\text{m}^2$$
$$\delta := I_2 + m_2 r_2^2 = 0.105\ \text{kg}\cdot\text{m}^2.$$

The state and input are $\eta := [\theta_1\ \theta_2\ \dot{\theta}_1\ \dot{\theta}_2]^\top$ and $\tau := [\tau_1\ \tau_2]^\top$, where τ_i is the torque applied to the base of link i.

A trajectory $\overline{\eta}$ of duration 5 s was selected for the tip of the arm to follow. This trajectory is shown as a solid black line in Figure 9. An equivalent trajectory in polar coordinates is also shown in Figure 10. The equilibrium input torque $\overline{\tau}$ can be computed using inverse kinematics. The robot should track this trajectory in the presence of small torque disturbances d_{in}. The input torque vector is $\tau = \overline{\tau} + u + d_{in}$ where u is an additional control torque to reject the disturbances. The nonlinear dynamics (28) are linearized around the trajectory $(\overline{\eta}, \overline{\tau})$ to obtain an LTV system H:

$$\dot{x}(t) = A(t)\,x(t) + B(t)\,(u(t) + d_{in}(t))\,, \tag{28}$$

where $x(t) := \eta(t) - \overline{\eta}(t)$ is the deviation from the equilibrium trajectory. An uncertain output feedback weighted interconnection of H is shown in the Figure 11. Let $\delta\theta := \begin{bmatrix} \delta\theta_1 \\ \delta\theta_2 \end{bmatrix}$ represent first-order perturbations in angular positions,

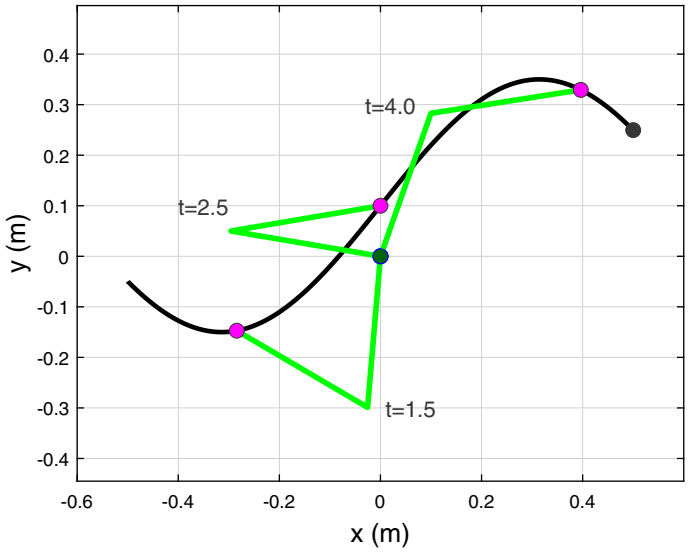

FIGURE 9 Snapshot positions in cartesian coordinates [Colour figure can be viewed at wileyonlinelibrary.com]

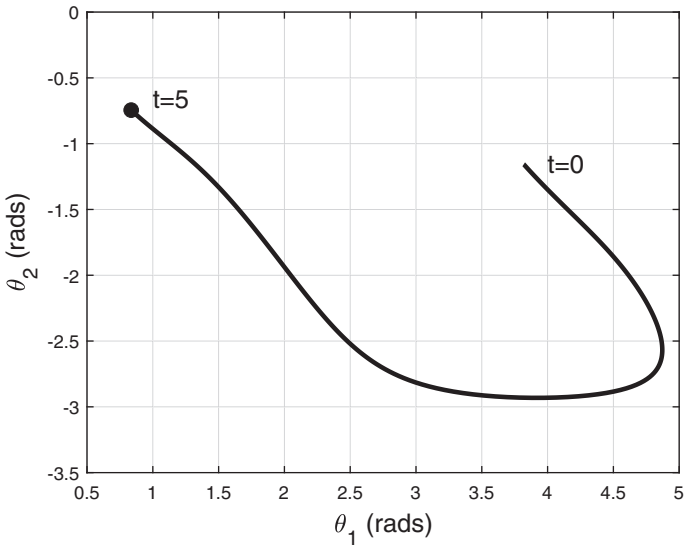

FIGURE 10 Nominal trajectory in polar coordinates

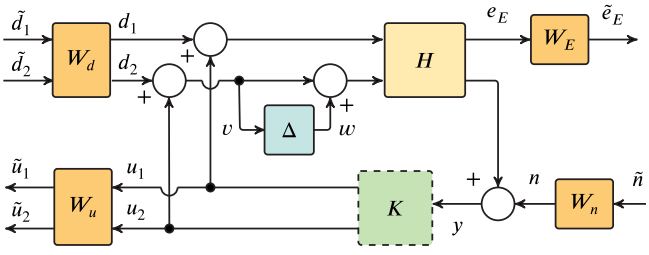

FIGURE 11 Uncertain output feedback weighted interconnection [Colour figure can be viewed at wileyonlinelibrary.com]

which is the output of interest e_E. The measurement is also $\delta\theta$ but corrupted by noise $n = \begin{bmatrix} n_1 \\ n_2 \end{bmatrix}$ and is fed to the controller as $y = \delta\theta + n$. The controller generates a commanded torque $u = \begin{bmatrix} u_1 \\ u_2 \end{bmatrix}$ is corrupted by input disturbance $d_{\text{in}} = \begin{bmatrix} d_1 \\ d_2 \end{bmatrix}$. The second control channel gets further corrupted by LTI input uncertainty Δ. The plant input perturbation Δ is a SISO LTI system with $\|\Delta\|_\infty \leq \beta$ where uncertainty level $\beta = 0.8$. This corresponds to the uncertainty set as discussed in Example 1. The synthesis objective is to minimize the closed-loop, worst-case gain from the generalized disturbance $\tilde{d} := \begin{bmatrix} \tilde{d}_{\text{in}} \\ \tilde{n} \end{bmatrix} = \begin{bmatrix} \tilde{d}_1 & \tilde{d}_2 & \tilde{n}_1 & \tilde{n}_2 \end{bmatrix}^\top$ to the generalized error $\tilde{e} := \begin{bmatrix} \tilde{u} \\ \tilde{e}_E \end{bmatrix}$. The weighted control effort $\tilde{u}$ is penalized in an

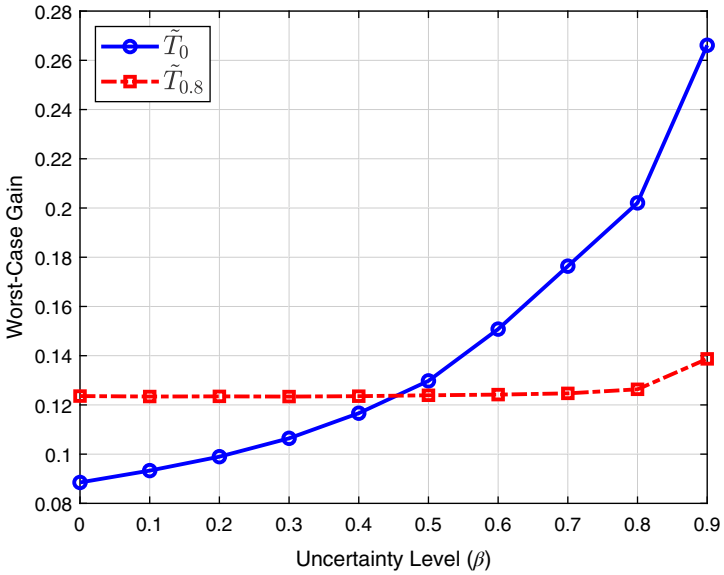

FIGURE 12 Worst-case gain comparison [Colour figure can be viewed at wileyonlinelibrary.com]

$\mathcal{L}_2[0, T]$ sense while $\tilde{e}_E$ is penalized with a terminal Euclidean norm at $T = 5$ s. Let $I_2 := \begin{bmatrix} 1 & 0 \\ 0 & 1 \end{bmatrix}$. The following (constant) design weights are chosen for the performance channels:

$$W_d = 0.1\, I_2, \quad W_n = 0.01\, I_2, \quad W_u = 0.5\, I_2, \quad W_E = I_2$$

The design weight associated with the uncertainty channels are not considered in this example, however, in general, the weights W_v and W_w can also be used for the respective uncertainty channels. As noted earlier, these design weights can be dynamic and/or time-varying. Let $\tilde{G}$ denote this weighted design interconnection for robust synthesis. It can be expressed in state-space form as in Equation (22). Algorithm 1 is run with $N_{\text{syn}} = 7$ iterations. No significant improvement is obtained after seventh iteration. The IQC analysis step is performed based on the approach in Reference 20 and using parameterization similar to Example 3 with $p = 10$, $q = 1$, $tol = 5 \times 10^{-3}$, $N_{\text{iter}} = 10$, t_{DLMI} as 20 and τ_{sp} as 10 evenly spaced grid points on the horizon $[0, 5]$ s.

Let $K_{0.8}$ denote the controller obtained at the end of the robust synthesis algorithm. This controller achieves the closed-loop worst-case performance of $\gamma_{0.8} = 0.126$. It took 11.7 hours to complete the seven iterations on a standard desktop computer with 3 GHz Core i7 processor. In addition, a nominal synthesis with $\Delta = 0$ was performed using the approach in Section 2.2. This controller, denoted as K_0, achieves a closed-loop nominal performance of $\gamma_0 = 0.089$. It took 49.8 seconds to perform this nominal synthesis. The corresponding uncertain closed-loops with the nominal and robust controllers are denoted by $\tilde{T}_0 := \mathcal{F}_u(\mathcal{F}_l(\tilde{G}, K_0), \Delta)$ and $\tilde{T}_{0.8} := \mathcal{F}_u(\mathcal{F}_l(\tilde{G}, K_{0.8}), \Delta)$. Figure 12 shows the worst-case performance versus the uncertainty level β for the uncertain closed-loops with these two controllers. The curve for $\tilde{T}_0$ (blue circles) has $\gamma = 0.089$ at $\beta = 0$ as reported above. The curve for $\tilde{T}_{0.8}$ (red squares) has $\gamma = 0.126$ at $\beta = 0.8$ as also reported above. This figure reveals the typical trade-off between performance and robustness. The nominal controller K_0 achieves better nominal performance ($\beta = 0$) than $K_{0.8}$. However, $K_{0.8}$ is more robust to higher levels of uncertainties.

Note that each data point in Figure 12 represents a worst-case gain induced from the generalized disturbance input $\tilde{d}$ to the generalized error output $\tilde{e}$. Both $\tilde{d}$ and $\tilde{e}$ have two components which can further be analyzed using induced gain for individual input–output pairs. Table 1 shows an analysis with no uncertainty (level $\beta = 0$) performed for the closed-loops with nominal control design $\tilde{T}_0$ (blue) and robust control design $\tilde{T}_{0.8}$ (red). It is evident that the induced gain from noise $\tilde{n}$ to control effort $\tilde{u}$ dominates the overall performance for both the interconnections. Moreover, the induced $\mathcal{L}_2$-gain from $\tilde{n}$ to $\tilde{u}$ for $\tilde{T}_{0.8}$ is 0.124 which is approximately 41% higher than the corresponding value for $\tilde{T}_0$ (=0.088). Likewise, the induced $\mathcal{L}_2$-to-Euclidean gain from disturbance $\tilde{d}_{in}$ to $\tilde{e}_E(T)$ is approximately 16.6% higher for $\tilde{T}_{0.8}$ (=0.077) as compared to $\tilde{T}_0$ (=0.066). The combined effect of the disturbance and noise is responsible for performance degradation of the robust controller at $\beta = 0$. Table 2 shows the worst-case gain upper bounds for robust analysis performed at an uncertainty level $\beta = 0.8$ for both interconnections. Note that the closed-loop with robust controller has the same worst-case induced $\mathcal{L}_2$-gain of 0.124 from $\tilde{n}$ to $\tilde{u}$ as in Table 1. Since, the robust controller explicitly accounts for model uncertainty, it has approximately 37.8% lower worst-case induced $\mathcal{L}_2$-gain from $\tilde{d}_{\text{in}}$ to $\tilde{u}$ compared to the nominal controller. Similarly, the

$\tilde{T}_0$ / $\tilde{T}_{0.8}$	Disturbance $\tilde{d}_{\text{in}}$	Measurement noise $\tilde{n}$	Generalized disturbance $\tilde{d}$
Euclidean output $\tilde{e}_E(T)$	0.066 / 0.077	0.050 / 0.047	0.082 / 0.081
Control effort $\tilde{u}$	0.085 / 0.087	0.088 / 0.124	0.089 / 0.124
Generalized error $\tilde{e}$	0.086 / 0.097	0.088 / 0.124	0.089 / 0.124

TABLE 1 Induced gain upper bounds for different input–output pairs (nominal analysis, $\beta = 0$)

$\tilde{T}_0$ / $\tilde{T}_{0.8}$	Disturbance $\tilde{d}_{\text{in}}$	Measurement noise $\tilde{n}$	Generalized disturbance $\tilde{d}$
Euclidean output $\tilde{e}_E(T)$	0.102 / 0.093	0.068 / 0.061	0.120 / 0.120
Control effort $\tilde{u}$	0.190 / 0.118	0.098 / 0.124	0.202 / 0.126
Generalized error $\tilde{e}$	0.190 / 0.118	0.106 / 0.125	0.202 / 0.126

TABLE 2 Worst-case gain upper bounds for different input–output pairs (robust analysis, $\beta = 0.8$)

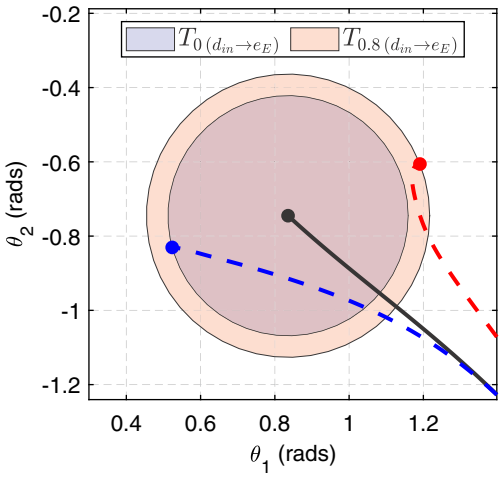

FIGURE 13 Nominal analysis ($\beta = 0$) [Colour figure can be viewed at wileyonlinelibrary.com]

robust controller performs better in terms of bounding the Euclidean outputs as compared to the nominal controller at $\beta = 0.8$. Overall, the disturbance rejection property for the nominal controller is degraded more from Tables 1 to 2 as compared to the robust controller. This observation is consistent with known frequency domain insights for infinite horizon LTI systems, as the high frequency noise rejection properties are typically less impacted by model uncertainties than the low frequency disturbance rejection properties.

As noted earlier, the primary design goal was to tightly bound the states at the final time $T = 5$ s. To study this further consider the impact of link joint disturbance d_{in} on the Euclidean output e_E. Let G denote the unweighted plant which has the same inputs/outputs as the weighted plant $\tilde{G}$ but with all weights set to identity. Further, let the respective uncertain interconnection using G be denoted as $T_0 := \mathcal{F}_u(\mathcal{F}_l(G, K_0), \Delta)$ and $T_{0.8} := \mathcal{F}_u(\mathcal{F}_l(G, K_{0.8}), \Delta)$. Nominal analysis performed for both the $T_{0\ (d_{in}\to e_E)}$ and $T_{0.8\ (d_{in}\to e_E)}$ interconnections gives both upper and lower bounds on the nominal performance. The upper bounds are obtained as 0.656 and 0.766, respectively, which are shown as blue and red disk in Figure 13 at the final time. The corresponding lower bounds are obtained as 0.648 and 0.763. The worst-case disturbance $\|d_{\text{in}}\|_{2,[0,T]} \leq 0.5$ for both interconnections are computed by solving the two point boundary value problem as presented in Reference 37. These specific bad disturbances (Figure 14) pushes the state trajectory (dashed line) as far as the computed lower bound in the LTV simulation.

A worst-case terminal Euclidean norm bound is computed for both the interconnections at the uncertainty level $\beta = 0.8$. The corresponding upper bound using the algorithm in Reference 20 was obtained as 1.02 and 0.93, respectively. This shows approximately a 8.82% reduction in Euclidean norm bound. As a graphical illustration, these bounds are depicted in Figure 15 as a disk at the final time $T = 5$ s. The bound accounts for all the disturbances d_{in} that satisfy $\|d_{\text{in}}\|_{2,[0,T]} \leq 0.5$ and all the LTI uncertainties Δ with norm bound $\beta = 0.8$.

To obtain a reasonable lower bound on the worst-case gain, first 100 uncertainties are sampled randomly as first order LTI systems with at most size 0.8. Then, uncertainty block Δ was replaced with each of sampled uncertainties and nominal

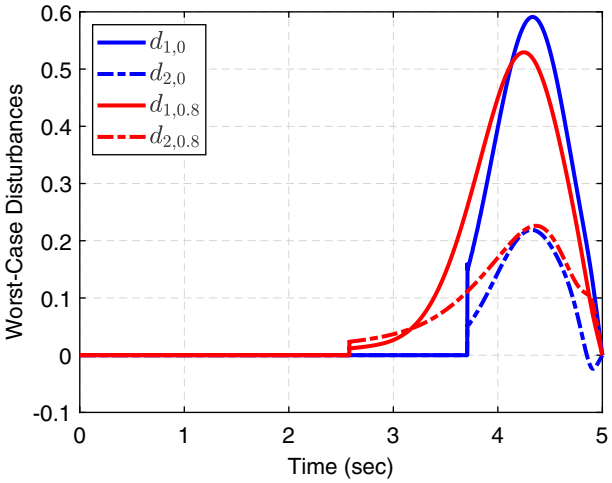

FIGURE 14 Worst-case disturbances [Colour figure can be viewed at wileyonlinelibrary.com]

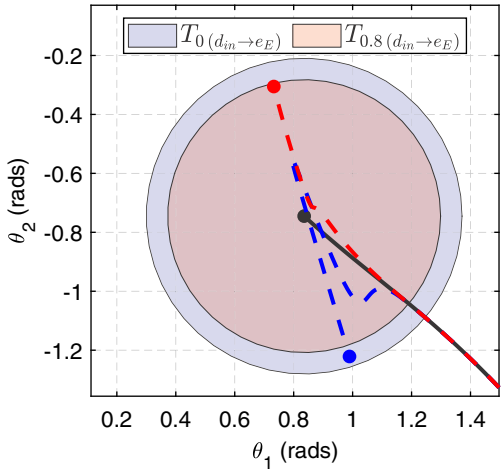

FIGURE 15 Robust analysis ($\beta = 0.8$) [Colour figure can be viewed at wileyonlinelibrary.com]

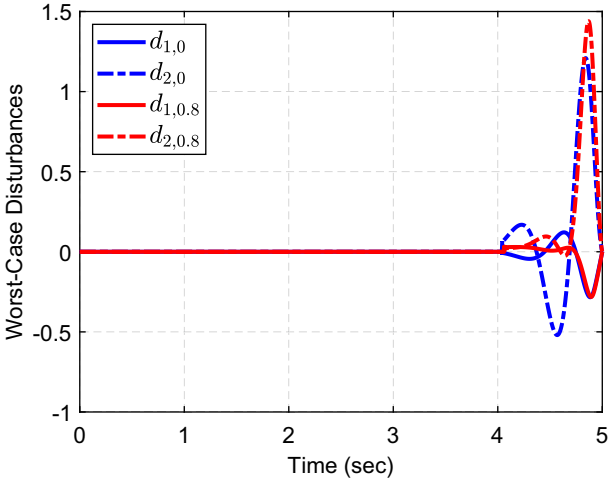

FIGURE 16 Worst-case disturbances [Colour figure can be viewed at wileyonlinelibrary.com]

LTV analysis was performed from d_{in} to e_E for both the interconnections. Worst-case uncertainties are then obtained after maximizing performance over the sample space. Let, the specific bad perturbation that yields to the poor performance for both $T_{0\ (d_{\text{in}}\to e_E)}$ and $T_{0.8\ (d_{\text{in}}\to e_E)}$ be denoted as Δ_{wc_1} and Δ_{wc_2} respectively.

$$\Delta_{wc_1} = \frac{-0.8\ s + 12.18}{s + 15.23}, \quad \Delta_{wc_2} = \frac{-0.8\ s + 25.89}{s + 32.36}$$

The worst-case gain lower bound corresponding to these perturbations are obtained as 1.001 and 0.903, respectively. It is evident that a combination of worst-case disturbance (Figure 16) (scaled to have size 0.5) and uncertainty (of size 0.8) pushes the states of the closed loop system (dashed line) as far as the lower bound of the worst-case gain. Overall, these simple comparison results show a typical robustness and performance trade-off. The nominal controller performs best at no uncertainty whereas the robust controller performs better at modeled uncertainty level.

6 | CONCLUSIONS AND FUTURE WORK

This paper proposed an iterative algorithm to design an output-feedback controller that bounds the worst-case gain of an uncertain LTV system on a finite horizon. Similar design can also be done in a state-feedback formulation. The performance was specified using both an induced $\mathcal{L}_2$ and terminal Euclidean norm penalty on the output. Time-domain dynamic IQCs were used to describe the input-output behavior of the uncertainty. The effectiveness of proposed approach was demonstrated using the two-link robot arm example.

This paper opens up few new directions for further research. First, we used a block diagonal assumption for the IQC filter and decision variables (Assumption 1). Future work will consider relaxing this assumption to include full block IQC multipliers in the robust synthesis. Second, note that the proposed method also allows time-varying uncertainty and performance weights. This is useful for many applications such as in many launch scenarios, where the uncertainty or performance requirements are not evenly spread out across the time horizon. Future work in this area is required to exploit the full potential of this method. Moreover, we recognize that proposed method is computationally expensive. Future research is needed to speed up the numerical computations for such finite horizon analysis and synthesis.

ACKNOWLEDGEMENTS

This work was gratefully supported by the US ONR grant N00014-18-1-2209. We would like to thank our collaborators Prof. Andrew Packard, Prof. Murat Arcak, and graduate students Kate Schweidel, Emmanuel Sin, Alex Devonport and Galaxy Yin for valuable discussions. We also thank Dr. Douglas Philbrick from U.S. Naval Air Warfare Center Weapons Division, China Lake for helpful comments. Finally, we thank Prof. Harald Pfifer for pointing out the technical issue with lemma 2 in earlier draft of this paper.

DATA AVAILABILITY STATEMENT

The data that support the findings of this study are openly available in LTVTools MATLAB toolbox at https://z.umn.edu/LTVTools, Reference 25.

ORCID

Jyot Buch https://orcid.org/0000-0002-1955-6338

REFERENCES

1. Subrahmanyam MB. *Finite Horizon* H_∞ *and Related Control Problems*. Berlin, Germany: Springer Science & Business Media; 2012.
2. Tucker MR. Continuous H_∞ and Discrete Time-varying Finite Horizon Robust Control with Industrial Applications [PhD Thesis]. University of Leicester; 1998.
3. Marcos A, Bennani S. LPV modeling, analysis and design in space systems: Rationale, objectives and limitations. Paper presented at: Proceedings of the AIAA Guidance, Navigation, and Control Conference, Chicago, Illinois; 2009; AIAA 2009-5633.
4. Biertümpfel F, Pifer H, Bennani S. Finite horizon worst case analysis of launch vehicles. *IFAC-PapersOnLine*. 2019;52(12):31-36.
5. Veenman J, Köroğlu H, Scherer C. Analysis of the controlled NASA HL20 atmospheric re-entry vehicle based on dynamic IQCs. Paper presented at: Proceedings of the AIAA Guidance, Navigation, and Control Conference, Chicago, Illinois; 2009; AIAA 2009–5637.
6. Doyle J, Lenz K, Packard A. Design examples using μ-synthesis: space shuttle lateral axis FCS during reentry. *Modelling, Robustness and Sensitivity Reduction in Control Systems*. New York, NY: Springer; 1987.

7. Balas G, Packard A. Design of robust, time-varying controllers for missile autopilots. Paper presented at: Proceedings of the first IEEE Conference on Control Applications, Dayton, Ohio; 1992:104-110.
8. Packard A, Doyle J, Balas G. Linear, multivariable robust control with a μ perspective. *J Dyn Syst Measur Control*. 1993;115(2B):426-438. https://doi.org/10.1115/1.2899083.
9. Veenman J, Scherer CW. IQC-synthesis with general dynamic multipliers. *Int J Robust Nonlinear Control*. 2014;24(17):3027-3056.
10. Petersen I, Ugrinovskii V, Savkin A. *Robust Control Design Using* H_∞ *Methods*. New York, NY: Springer; 2000.
11. Green M, Limebeer DJ. *Linear Robust Control*. Chelmsford, MA: Courier Corporation; 2012.
12. Tadmor G. Worst-case design in the time domain: the maximum principle and the standard H_∞ problem. *Math Control Signals Syst*. 1990;3(4):301-324.
13. Limebeer DJ, Anderson BD, Khargonekar PP, Green M. A game theoretic approach to H_∞ control for time-varying systems. *SIAM J Control Optim*. 1992;30(2):262-283.
14. Khargonekar PP, Nagpal KM, Poolla KR. H_∞ control with transients. *SIAM J Control Optim*. 1991;29(6):1373-1393.
15. Ravi R, Nagpal KM, Khargonekar PP. H_∞ control of linear time-varying systems: a state-space approach. *SIAM J Control Optim*. 1991;29(6):1394-1413.
16. Uchida K, Fujita M. Finite horizon H_∞ control problems with terminal penalties. *IEEE Trans Automat Control*. 1992;37(11):1762-1767.
17. Lall S, Glover K. Riccati differential inequalities: suboptimal H_∞ controllers for finite horizon time varying systems. Paper presented at: Proceedings of 1995 34th IEEE Conference on Decision and Control, New Orleans, Louisiana, vol. 1, 1995:955-956.
18. Yakubovich V. Frequency conditions for the absolute stability of control systems with several nonlinear or linear nonstationary blocks. *Avtomatika i telemekhanika*. 1967;6:5-30.
19. Megretski A, Rantzer A. System analysis via integral quadratic constraints. *IEEE Trans Automat Control*. 1997;42(6):819-830.
20. Seiler P, Moore RM, Meissen C, Arcak M, Packard A. Finite horizon robustness analysis of LTV systems using integral quadratic constraints. *Automatica*. 2019;100:135-143.
21. Wang S, Pfifer H, Seiler P. Robust synthesis for linear parameter varying systems using integral quadratic constraints. *Automatica*. 2016;68:111-118.
22. Veenman J, Scherer CW. On robust LPV controller synthesis: a dynamic integral quadratic constraint based approach. Paper presented at: Proceedings of the49th IEEE Conference on Decision and Control (CDC), Atlanta, Georgia; 2010:591-596.
23. O'rien R Jr, Iglesias PA. Robust controller design for linear, time-varying systems. *Europ J Control*. 1999;5(2-4):222-241.
24. Pirie C, Dullerud GE. Robust controller synthesis for uncertain time-varying systems. *SIAM J Control Optim*. 2002;40(4):1312-1331.
25. Seiler P, Buch J, Moore RM, Meissen C, Arcak M, Packard A. LTVTools (beta), A MATLAB toolbox for linear time-varying systems; 2018.
26. Buch J, Seiler P. Finite horizon robust synthesis. Paper presented at: Proceedings of the Accepted to American Control Conference, Denver, Colorado: IEEE; 2020.
27. Zhou K, Doyle JC, Glover K. *Robust and Optimal Control*. Upper Saddle River, NJ: Prentice Hall; 1996.
28. Dullerud GE, Paganini FA. *Course in Robust Control Theory: A Convex Approach*. Vol 36. Berlin, Germany: Springer Science & Business Media; 2013.
29. Pfifer H, Seiler P. Robustness analysis with parameter-varying integral quadratic constraints. Paper presented at: Proceedings of the American Control Conference (ACC), Chicago, Illinois: IEEE; 2015:138-143.
30. Balakrishnan V. Lyapunov functionals in complex μ analysis. *IEEE Trans Automat Control*. 2002;47(9):1466-1479.
31. Veenman J, Scherer CW, Köroğlu H. Robust stability and performance analysis based on integral quadratic constraints. *Europ J Control*. 2016;31:1-32.
32. Seiler P. Stability analysis with dissipation inequalities and integral quadratic constraints. *IEEE Trans Automat Control*. 2014;60(6):1704-1709.
33. Willems JC. Dissipative dynamical systems part I: general theory. *Arch Ration Mech Anal*. 1972;45(5):321-351.
34. van der Schaft A. *L_2 gain and Passivity in Nonlinear Control*. Berlin, Germany: Springer-Verlag; 1999.
35. Khalil H. *Nonlinear Systems*. 3rd ed. Upper Saddle River, NJ: Prentice Hall; 2001.
36. Murray R, Li Z, Sastry S. *A Mathematical Introduction to Robot Manipulation*. Boca Raton, FL: CRC Press; 1994.
37. Iannelli A, Seiler P, Marcos A. Worst-case disturbances for time-varying systems with application to flexible aircraft. *J Guid Control Dyn*. 2019;42(6):1261-1271.
38. Francis B. A course in H_∞ control theory. *Lect Notes Control Inf Sci*. 1987;88:R5.
39. Molinari B. Nonnegativity of a quadratic functional. *SIAM J Control*. 1975;13(4):792-806.
40. Kučera V. A review of the matrix Riccati equation. *Kybernetika*. 1973;9(1):42-61.

How to cite this article: Buch J, Seiler P. Finite horizon robust synthesis using integral quadratic constraints. *Int J Robust Nonlinear Control*. 2021;31:3011–3035. https://doi.org/10.1002/rnc.5431

APPENDIX A. GENERIC QUADRATIC COST

This paper considers an induced norm $\|H\|_{[0,T]}$ (defined by Equation (4)) as a performance metric whereas a generic quadratic cost is considered in Reference 20. This appendix describes the equivalence between these two formulations. First, consider the finite-horizon linear quadratic optimal control problem as follows:

$$J^*(\gamma) := \sup_{0\neq d\in\mathcal{L}_2[0,T]} x(T)^\top F x(T) + \int_0^T \begin{bmatrix} x(t) \\ d(t) \end{bmatrix}^\top \begin{bmatrix} Q(t) & S(t) \\ S(t)^\top & R(t,\gamma) \end{bmatrix} \begin{bmatrix} x(t) \\ d(t) \end{bmatrix} dt$$
$$\text{s.t. } \dot{x}(t) = A(t)\,x(t) + B(t)\,d(t) \text{ and } x(0) = 0. \tag{A1}$$

where $Q : [0,T] \to \mathbb{S}^{n_x}$, $S : [0,T] \to \mathbb{R}^{n_x \times n_d}$, $R : [0,T] \oplus \mathbb{R}^+ \to \mathbb{S}^{n_d}$ and $F \in \mathbb{R}^{n_x \times n_x}$. We assume $Q(t) \succcurlyeq 0$, for all $t \in [0,T]$ and $F \succcurlyeq 0$. Moreover, we assume a form $R(t,\gamma) = R_0(t) - \gamma^2 I_{n_d}$, where $\gamma > 0$, $R_0(t) \succcurlyeq 0$ and $R(t,\gamma) \prec 0$, for all $t \in [0,T]$. There are two directions to the equivalence. First, assume a system H is given as defined by Equation (1) and (3). Note that the induced norm $\|H\|_{[0,T]}$ is defined by the state-space matrices (A, B, C_I, C_E, D_I). Define (Q, S, R, F) as in Theorem 1. Then for any $\gamma > 0$, $\|H\|_{[0,T]} < \gamma$ if and only if $J^*(\gamma) < 0$. This is shown in section 2 of Reference 20. Conversely, assume the generic quadratic cost defined by Equation (A1) is given with cost matrices (Q, S, R, F) satisfying the assumptions above. If we further assume that $Q(t) - S(t)R_0(t)^{-1}S(t)^\top \succ 0$ then we can perform the following factorization:

$$\begin{bmatrix} Q(t) & S(t) \\ S(t)^\top & R_0(t) \end{bmatrix} = \begin{bmatrix} C_I(t)^\top \\ D_I(t)^\top \end{bmatrix} \begin{bmatrix} C_I(t) & D_I(t) \end{bmatrix}, \tag{A2}$$

In addition, define $C_E := F^{\frac{1}{2}}$. Then the generic quadratic cost is rewritten as:

$$J^*(\gamma) = \sup_{0\neq d\in\mathcal{L}_2[0,T]} e_E(T)^\top e_E(T) + \int_0^T e_I(t)^\top e_I(t)\,dt - \gamma^2 \int_0^T d(t)^\top\,d(t)\,dt$$
$$\text{s.t. Equation (1), (3), and } x(0) = 0. \tag{A3}$$

This cost satisfies $J^*(\gamma) < 0$ if and only if $\|H\|_{[0,T]} < \gamma$.

APPENDIX B. FINITE HORIZON FACTORIZATION

For infinite horizon LTI systems, spectral factorization results are found in standard robust control textbooks.[27,28,38] The following lemma provides a time-varying finite horizon generalization of this result.

Lemma 2. *Consider an LTV system $\Psi : \mathcal{L}_2^{n_d}[0,T] \to \mathcal{L}_2^{n_e}[0,T]$ be given with state-space realization as follows:*

$$\begin{aligned} \dot{x}(t) &= A(t)\,x(t) + B(t)\,d(t) \\ e(t) &= C(t)\,x(t) + D(t)\,d(t), \end{aligned} \tag{B1}$$

with $x \in \mathbb{R}^{n_x}$, $e \in \mathbb{R}^{n_e}$, $d \in \mathbb{R}^{n_d}$ and $D(t)$ is full column rank $\forall t \in [0,T]$. Let $M : [0,T] \to \mathbb{S}^{n_e}$ be a given piecewise continuous matrix valued function with $M(t) \succ 0, \forall\, t \in [0,T]$. Let $Q : [0,T] \to \mathbb{S}^{n_x}$, $S : [0,T] \to \mathbb{R}^{n_x \times n_d}$, $R : [0,T] \to \mathbb{S}^{n_d}$ be defined as follows.

$$Q := C^\top M C, \quad S := C^\top M D, \quad R := D^\top M D, \tag{B2}$$

with $R(t) \succ 0, \forall\, t \in [0,T]$. The following statements hold.

1. *There exist a differentiable function $X : [0,T] \to \mathbb{S}^n$ such that $X(T) = 0$ and*

$$\dot{X} + A^\top X + XA + Q - (XB + S)R^{-1}(XB + S)^\top = 0, \tag{B3}$$

2. $\Phi := \Psi^{\sim} M \Psi$ *has a finite horizon factorization* $\Phi = U^{\sim} U$ *where* U *is square invertible LTV system defined on* $[0, T]$ *with the following state-space realization:*

$$U = \left[\begin{array}{c|c} A & B \\ \hline W^{-T}(B^{\top} X + S^{\top}) & W \end{array}\right], \tag{B4}$$

where $R(t) = W(t)^{\top} W(t)$, $\forall t \in [0, T]$.

Proof. Since $R(t) \succ 0$ and by Schur complement lemma $Q(t) - S(t)R(t)^{-1}S(t)^{\top} \succ 0, \forall\, t \in [0, T]$, the RDE does not have a finite escape time and thus always have a bounded unique solution regardless of the boundary condition (corollary 2.3 of Reference 39, theorem 8 in Reference 40). Further, it can be verified that the time-varying state-space realization of $\Psi^{\sim} M \Psi$ is related to that of a system $U^{\sim} U$ by a similarity transformation matrix $\begin{bmatrix} I & 0 \\ X(t) & I \end{bmatrix}$. ∎

APPENDIX C. PROOF OF LEMMA 1

Lemma 3. *Let* $\epsilon > 0$, $\gamma > 0$, $M_v(t) \succ 0$, $M_w(t) \succ 0$ *and a differentiable function* $P : [0, T] \to \mathbb{S}^n$ *such that* $P(T) \geq F$ *be given with the choice of* (Q, S, R, F) *as in Equation (14). The following statements are equivalent:*

1. $\mathrm{DLMI}_{\mathrm{Rob}}(P, M, \gamma^2, t) \leq -\epsilon I, \quad \forall t \in [0, T]$.
2. $\|N_{\mathrm{scl}}\|_{[0,T]} \leq 1 - \hat{\epsilon}$, *for some* $\hat{\epsilon}$.

Proof. **(1 ⇒ 2)** This proof is presented in two parts. First, we show that $\mathrm{DLMI}_{\mathrm{Rob}}(P, M, \gamma^2, t) \leq -\epsilon I,\ \forall t \in [0, T]$ can equivalently be written as a dissipation inequality with only single valid IQC. Second, the state-space realization of the extended system N_{ext} and the scaled system N_{scl} are indeed the same, which allow us to rewrite the robust performance DLMI as a nominal performance DLMI for N_{scl}. Integrating the related dissipation inequality completes the proof.

Part (i): Define a storage function $V(x, t) := x^{\top} P(t) x$. Left and right multiply the DLMI (13) by $[x^{\top}, w^{\top}, d^{\top}]$ and its transpose to show that V satisfies the following dissipation inequality for all $t \in [0, T]$:

$$\dot{V} + \left[\begin{bmatrix} x \\ \begin{bmatrix} w \\ d \end{bmatrix} \end{bmatrix}^{\top} \begin{bmatrix} Q & S \\ S^{\top} & R \end{bmatrix} \left[\begin{bmatrix} x \\ \begin{bmatrix} w \\ d \end{bmatrix} \end{bmatrix} + z^{\top} M z \leq -\epsilon\ d^{\top} d, \right. \tag{C1}$$

where $x = \begin{bmatrix} x_N \\ x_{\psi} \end{bmatrix} \in \mathbb{R}^n$ is the state of extended system as shown in Figure 4. Consider the outputs of the IQC filter $\Psi = \begin{bmatrix} \Psi_v & 0 \\ 0 & \Psi_w \end{bmatrix}$ be partitioned as $z := \begin{bmatrix} z_v \\ z_w \end{bmatrix}$. Let Ψ_v have the following state-space representation with state x_v, input v, and output z_v:

$$\begin{aligned} \dot{x}_v(t) &= A_1(t)\, x_v(t) + B_1(t)\, v(t) \\ z_v(t) &= C_1(t)\, x_v(t) + D_1(t)\, v(t). \end{aligned} \tag{C2}$$

A similar time-varying state-space expression also holds for Ψ_w with matrices (A_2, B_2, C_2, D_2), state x_w, input w, and output z_w. Thus the term $z^{\top} M z$ in (C1) can be expressed as:

$$\begin{aligned} z^{\top} M z &= z_v^{\top} M_v z_v - z_w^{\top} M_w z_w \\ &= \begin{bmatrix} x_v \\ v \end{bmatrix}^{\top} \begin{bmatrix} C_1^{\top} \\ D_1^{\top} \end{bmatrix} M_v \begin{bmatrix} C_1 & D_1 \end{bmatrix} \begin{bmatrix} x_v \\ v \end{bmatrix} - \begin{bmatrix} x_w \\ w \end{bmatrix}^{\top} \begin{bmatrix} C_2^{\top} \\ D_2^{\top} \end{bmatrix} M_w \begin{bmatrix} C_2 & D_2 \end{bmatrix} \begin{bmatrix} x_w \\ w \end{bmatrix}. \end{aligned} \tag{C3}$$

First, consider only the terms involving v and define the quadratic storage matrices as:

$$\begin{bmatrix} Q_v & S_v \\ S_v^\top & R_v \end{bmatrix} := \begin{bmatrix} C_1^\top \\ D_1^\top \end{bmatrix} M_v \begin{bmatrix} C_1 & D_1 \end{bmatrix}. \tag{C4}$$

By Lemma 2 in Appendix B, the condition $M_v(t) \succ 0, \forall t \in [0, T]$ implies that there exists $X_v : [0, T] \to \mathbb{S}^{n_{x_v}}$ such that:

$$\dot{X}_v + A_1^\top X_v + X_v A_1 + Q_v - (X_v B_1 + S_v) R_v^{-1} (X_v B_1 + S_v)^\top = 0, \quad X_v(T) = 0. \tag{C5}$$

Moreover, Lemma 2 in Appendix B also implies that there exists a spectral factor U_v with a state-space realization as $(A_1, B_1, \tilde{C}_1, \tilde{D}_1)$ with $\tilde{C}_1 := W_v^{-T}(B_1^\top X_v + S_v^\top)$, $\tilde{D}_1 := W_v$ and $R_v = W_v^\top W_v$. Note that x_v is the state and $\tilde{v}$ is the output of the spectral factor U_v. The RDE (C5) can be written in terms of the state matrices of U_v as:

$$Q_v = -\dot{X}_v - A_1^\top X_v - X_v A_1 + \tilde{C}_1^\top \tilde{C}_1. \tag{C6}$$

Substitute above Q_v and $S_v^\top = \tilde{D}_1^\top \tilde{C}_1 - B_1^\top X_v$ in (C4) to obtain the following expression:

$$z_v^\top M_v z_v = -x_v \dot{X}_v x_v - (A_1 x_v + B_1 v)^\top X_v x_v - x_v^\top X_v (A_1 x_v + B_1 v) + (\tilde{C}_1 x_v + \tilde{D}_1 v)^\top (\tilde{C}_1 x_v + \tilde{D}_1 v). \tag{C7}$$

This can be simplified to the following expression:

$$z_v^\top M_v z_v = -x_v^\top \dot{X}_v x_v - \dot{x}_v^\top X_v x_v - x_v^\top X_v \dot{x}_v + \tilde{v}^\top \tilde{v} = -\frac{d}{dt}\left(x_v^\top X_v x_v\right) + \tilde{v}^\top \tilde{v}. \tag{C8}$$

Similarly, with $M_w(t) \succ 0, \forall t \in [0, T]$ the spectral factor U_w can be obtained with a state-space realization $(A_2, B_2, \tilde{C}_2, \tilde{D}_2)$, states x_w, and outputs $\tilde{w}$. The following expression holds:

$$z_w^\top M_w z_w = -\frac{d}{dt}\left(x_w^\top X_w x_w\right) + \tilde{w}^\top \tilde{w}, \tag{C9}$$

where $X_w : [0, T] \to \mathbb{S}^{n_{x_w}}$ is a solution to a related RDE with respective quadratic storage matrices and the boundary condition $X_w(T) = 0$. Subtract Equation (C9) from (C8) to get the left-hand side of the Equation (C3) as follows:

$$z^\top M z \quad = -\tfrac{d}{dt}\left(x_\psi^\top X x_\psi\right) + \tilde{v}^\top \tilde{v} - \tilde{w}^\top \tilde{w}, \tag{C10}$$

where $x_\psi = \begin{bmatrix} x_v \\ x_w \end{bmatrix}$, $X(t) := \begin{bmatrix} X_v(t) & 0 \\ 0 & -X_w(t) \end{bmatrix}$ and $X(T) = 0$. Let the modified matrix $\tilde{P}(t)$ be defined as follows:

$$\tilde{P}(t) := P(t) - \begin{bmatrix} 0 & 0 \\ 0 & X(t) \end{bmatrix}. \tag{C11}$$

This yields a modified storage function $\tilde{V}(x, t) := x^\top \tilde{P}(t) x$. The modified storage function has the form:

$$\tilde{V}(x, t) = V(x, t) - x_v^\top X_v x_v + x_w^\top X_w x_w, \tag{C12}$$

where the second and third term can be interpreted as hidden energy stored in the IQC multiplier. With modified storage function $\tilde{V}$ the dissipation inequality (C1) can be recast as,

$$\dot{\tilde{V}} + \begin{bmatrix} x \\ \begin{bmatrix} w \\ d \end{bmatrix} \end{bmatrix}^\top \begin{bmatrix} Q & S \\ S^\top & R \end{bmatrix} \begin{bmatrix} x \\ \begin{bmatrix} w \\ d \end{bmatrix} \end{bmatrix} + \begin{bmatrix} \tilde{v} \\ \tilde{w} \end{bmatrix}^\top J_{n_v, n_w} \begin{bmatrix} \tilde{v} \\ \tilde{w} \end{bmatrix} \leq -\epsilon \, d^\top d. \tag{C13}$$

This dissipation inequality is equivalent to (C1) with a single IQC $\mathcal{I}(U, J_{n_v,n_w})$ where $U := \begin{bmatrix} U_v & 0 \\ 0 & U_w \end{bmatrix}$. Next, We show that $\mathcal{I}(U, J_{n_v,n_w})$ is a valid time-domain IQC. To see this, define $V_\psi(x_\psi(t), t) := x_\psi(t)^\top X(t) x_\psi(t)$, $\tilde{z}(t) := \begin{bmatrix} \tilde{v}(t) \\ \tilde{w}(t) \end{bmatrix}$ and integrate Equation (C10) both sides from 0 to T to obtain:

$$\int_0^T z^\top M z \, dt = -V_\psi(x_\psi(T), T) + V_\psi(x_\psi(0), 0) + \int_0^T \tilde{z}^\top J_{n_v,n_w} \tilde{z} \, dt. \tag{C14}$$

Note that $V_\psi(x_\psi(0), 0) = 0$ because $x_\psi(0) = 0$ and $V_\psi(x_\psi(T), T) = x_\psi(T)^\top X(T) x_\psi(T) = 0$ due to the boundary condition $X(T) = 0_{n_\psi}$ of the time-varying factorization RDE. Thus if $\int_0^T z^\top M z \, dt \geq 0$ then we have $\int_0^T \tilde{z}^\top J_{n_v,n_w} \tilde{z} \, dt \geq 0$. Finally, note that $\tilde{P}(t)$ satisfies the same boundary condition as $P(t)$, that is, $\tilde{P}(T) \geq F$ because of the boundary condition $X(T) = 0$. Thus, $\tilde{V}(x, t)$ is a valid storage function $\forall t \in [0, T]$.

Part (ii): Let the extended system of N with spectral factor U be written in partitioned form as:

$$\left[\begin{array}{c} \dot{x} \\ \hline \tilde{v} \\ \tilde{w} \\ e_I \\ e_E \end{array}\right] = \left[\begin{array}{c|cc} \mathcal{A} & \mathcal{B}_w & \mathcal{B}_d \\ \hline \mathcal{C}_{\tilde{v}} & \mathcal{D}_{\tilde{v}w} & \mathcal{D}_{\tilde{v}d} \\ \mathcal{C}_{\tilde{w}} & \mathcal{D}_{\tilde{w}w} & 0 \\ \mathcal{C}_I & \mathcal{D}_{Iw} & \mathcal{D}_{Id} \\ \mathcal{C}_E & 0 & 0 \end{array}\right] \left[\begin{array}{c} x \\ \hline w \\ d \end{array}\right], \tag{C15}$$

where $x = \begin{bmatrix} x_N \\ x_v \\ x_w \end{bmatrix} \in \mathbb{R}^n$ and state-space matrices:

$$\mathcal{A} := \begin{bmatrix} A_N & 0 & 0 \\ B_1 C_v & A_1 & 0 \\ 0 & 0 & A_2 \end{bmatrix}, \mathcal{B}_w := \begin{bmatrix} B_w \\ B_1 D_{vw} \\ B_2 \end{bmatrix}, \mathcal{B}_d := \begin{bmatrix} B_d \\ B_1 D_{vd} \\ 0 \end{bmatrix}$$

$$\mathcal{C}_{\tilde{v}} := \begin{bmatrix} \tilde{D}_1 C_v & \tilde{C}_1 & 0 \end{bmatrix}, \mathcal{C}_I := \begin{bmatrix} C_I & 0 & 0 \end{bmatrix}, \mathcal{C}_{\tilde{w}} := \begin{bmatrix} 0 & 0 & \tilde{C}_2 \end{bmatrix}$$

$$\mathcal{C}_E := \begin{bmatrix} C_E & 0 & 0 \end{bmatrix}, \mathcal{D}_{\tilde{v}w} := \tilde{D}_1 D_{vw}, \mathcal{D}_{\tilde{v}d} := \tilde{D}_1 D_{vd}$$

$$\mathcal{D}_{\tilde{w}w} := \tilde{D}_2, \mathcal{D}_{Iw} := D_{Iw}, \mathcal{D}_{Id} = D_{Id}.$$

Using the choice of (Q, S, R) from Equation (14), the following partitioned DLMI is equivalent to the dissipation inequality (C13) for the state-space realization of (C15).

$$\begin{bmatrix} \dot{\tilde{P}} + \mathcal{A}^\top \tilde{P} + \tilde{P} \mathcal{A} & \tilde{P} \mathcal{B}_w & \tilde{P} \mathcal{B}_d \\ \mathcal{B}_w^\top \tilde{P} & 0_{n_w} & 0 \\ \mathcal{B}_d^\top \tilde{P} & 0 & -\gamma^2 I_{n_d} \end{bmatrix} + \begin{bmatrix} \mathcal{C}_I^\top \\ \mathcal{D}_{Iw}^\top \\ \mathcal{D}_{Id}^\top \end{bmatrix} \begin{bmatrix} \mathcal{C}_I & \mathcal{D}_{Iw} & \mathcal{D}_{Id} \end{bmatrix} + \begin{bmatrix} \mathcal{C}_{\tilde{v}}^\top & \mathcal{C}_{\tilde{w}}^\top \\ \mathcal{D}_{\tilde{v}w}^\top & \mathcal{D}_{\tilde{w}w}^\top \\ \mathcal{D}_{\tilde{v}d} & 0 \end{bmatrix} J_{n_v,n_w} \begin{bmatrix} \mathcal{C}_{\tilde{v}} & \mathcal{D}_{\tilde{v}w} & \mathcal{D}_{\tilde{v}d} \\ \mathcal{C}_{\tilde{w}} & \mathcal{D}_{\tilde{w}w} & 0 \end{bmatrix} \leq -\epsilon I. \tag{C16}$$

The condition $M_w(t) \succ 0, \forall t \in [0, T]$ is sufficient to ensure that $\mathcal{D}_{\tilde{w}w} := \tilde{D}_2$ is nonsingular. The output equation for w can be written as: $w = \mathcal{D}_{\tilde{w}w}^{-1}(\tilde{w} - \mathcal{C}_{\tilde{w}} x)$. Use this relation to substitute for w in Equation (C15). This gives the following scaled system:

$$\left[\begin{array}{c} \dot{x} \\ \hline \tilde{v} \\ e_I \\ e_E \end{array}\right] = \left[\begin{array}{c|cc} \mathcal{A} & \mathcal{B}_w & \mathcal{B}_d \\ \hline \mathcal{C}_{\tilde{v}} & \mathcal{D}_{\tilde{v}w} & \mathcal{D}_{\tilde{v}d} \\ \mathcal{C}_I & \mathcal{D}_{Iw} & \mathcal{D}_{Id} \\ \mathcal{C}_E & 0 & 0 \end{array}\right] L \left[\begin{array}{c} x \\ \hline \tilde{w} \\ d \end{array}\right], \tag{C17}$$

where the nonsingular time-varying matrix L is defined as:

$$L := \begin{bmatrix} I_n & 0 & 0 \\ -\mathcal{D}_{\tilde{w}w}^{-1}\mathcal{C}_{\tilde{w}} & \mathcal{D}_{\tilde{w}w}^{-1} & 0 \\ 0 & 0 & I_{n_d} \end{bmatrix}. \tag{C18}$$

Equation (C17) can be rewritten as follows:

$$\left[\begin{array}{c} \dot{x} \\ \hline \tilde{v} \\ e_I \\ e_E \end{array}\right] = \left[\begin{array}{c|cc} \tilde{\mathcal{A}} & \mathcal{B}_{\tilde{w}} & \mathcal{B}_d \\ \hline \tilde{\mathcal{C}}_{\tilde{v}} & \mathcal{D}_{\tilde{v}\tilde{w}} & \mathcal{D}_{\tilde{v}d} \\ \tilde{\mathcal{C}}_I & \mathcal{D}_{I\tilde{w}} & \mathcal{D}_{Id} \\ \mathcal{C}_E & 0 & 0 \end{array}\right] \left[\begin{array}{c} x \\ \hline \tilde{w} \\ d \end{array}\right], \tag{C19}$$

where the updated state-space matrices are defined as:

$$\begin{aligned} \tilde{\mathcal{A}} &:= \begin{bmatrix} A_N & 0 & -B_w\tilde{D}_2^{-1}\tilde{C}_2 \\ B_1C_v & A_1 & -B_1D_{vw}\tilde{D}_2^{-1}\tilde{C}_2 \\ 0 & 0 & A_2 - B_2\tilde{D}_2^{-1}\tilde{C}_2 \end{bmatrix}, \ \mathcal{B}_{\tilde{w}} := \begin{bmatrix} B_w\tilde{D}_2^{-1} \\ B_1D_{vw}\tilde{D}_2^{-1} \\ B_2\tilde{D}_2^{-1} \end{bmatrix} \\ \tilde{\mathcal{C}}_{\tilde{v}} &= \begin{bmatrix} \tilde{D}_1C_v & \tilde{C}_1 & -\tilde{D}_1D_{vw}\tilde{D}_2^{-1}\tilde{C}_2 \end{bmatrix}, \ \tilde{\mathcal{C}}_I := \begin{bmatrix} C_I & 0 & -D_{Iw}\tilde{D}_2^{-1}\tilde{C}_2 \end{bmatrix} \\ \mathcal{D}_{\tilde{v}\tilde{w}} &:= \tilde{D}_1D_{vw}\tilde{D}_2^{-1}, \ \mathcal{D}_{I\tilde{w}} := D_{Iw}\tilde{D}_2^{-1}. \end{aligned}$$

Note that the following state-space matrices of the inverse system of U_w shows up in the above representation.

$$U_w^{-1} := \left[\begin{array}{c|c} A_2 - B_2\tilde{D}_2^{-1}\tilde{C}_2 & B_2\tilde{D}_2^{-1} \\ \hline -\tilde{D}_2^{-1}\tilde{C}_2 & \tilde{D}_2^{-1} \end{array}\right]. \tag{C20}$$

Let scaled signal $\tilde{d} := \gamma\, d$ and state-space matrices $(\mathcal{A}_{\text{scl}}, \mathcal{B}_{\text{scl}}, \mathcal{C}_{\text{scl}}, \mathcal{D}_{\text{scl}})$ be defined as follows:

$$\mathcal{A}_{\text{scl}} := \tilde{\mathcal{A}}, \quad \mathcal{B}_{\text{scl}} := \begin{bmatrix} \mathcal{B}_{\tilde{w}} & \gamma^{-1}\mathcal{B}_d \end{bmatrix}, \quad \mathcal{C}_{\text{scl}} := \begin{bmatrix} \tilde{\mathcal{C}}_{\tilde{v}} \\ \tilde{\mathcal{C}}_I \end{bmatrix}, \quad \mathcal{D}_{\text{scl}} := \begin{bmatrix} \tilde{D}_1D_{vw}\tilde{D}_2^{-1} & \gamma^{-1}\tilde{D}_1D_{vd} \\ D_{Iw}\tilde{D}_2^{-1} & \gamma^{-1}D_{Id} \end{bmatrix}. \tag{C21}$$

It is readily verified that, with above definition, the scaled plant N_{scl} has a state-space realization as follows:

$$\left[\begin{array}{c} \dot{x} \\ \hline \begin{bmatrix} \tilde{v} \\ e_I \end{bmatrix} \\ e_E \end{array}\right] = \left[\begin{array}{c|c} \mathcal{A}_{\text{scl}} & \mathcal{B}_{\text{scl}} \\ \hline \mathcal{C}_{\text{scl}} & \mathcal{D}_{\text{scl}} \\ \mathcal{C}_E & 0 \end{array}\right] \left[\begin{array}{c} x \\ \hline \begin{bmatrix} \tilde{w} \\ \tilde{d} \end{bmatrix} \end{array}\right]. \tag{C22}$$

Perform the congruence transformation by multiplying the DLMI (C16) on the left/right by $L^\top/L$ to get:

$$\begin{bmatrix} \dot{\tilde{P}} + \tilde{\mathcal{A}}^\top\tilde{P} + \tilde{P}\tilde{\mathcal{A}} & \tilde{P}\mathcal{B}_{\tilde{w}} & \tilde{P}\mathcal{B}_d \\ \mathcal{B}_{\tilde{w}}^\top\tilde{P} & 0_{n_{\tilde{w}}} & 0 \\ \mathcal{B}_d^\top\tilde{P} & 0 & -\gamma^2 I_{n_d} \end{bmatrix} + \begin{bmatrix} \tilde{\mathcal{C}}_I^\top \\ \mathcal{D}_{I\tilde{w}}^\top \\ \mathcal{D}_{Id}^\top \end{bmatrix} \begin{bmatrix} \tilde{\mathcal{C}}_I & \mathcal{D}_{I\tilde{w}} & \mathcal{D}_{Id} \end{bmatrix} + \begin{bmatrix} \tilde{\mathcal{C}}_{\tilde{v}}^\top & 0 \\ \mathcal{D}_{\tilde{v}\tilde{w}}^\top & I_{n_{\tilde{w}}} \\ \mathcal{D}_{\tilde{v}d}^\top & 0 \end{bmatrix} J \begin{bmatrix} \tilde{\mathcal{C}}_{\tilde{v}} & \mathcal{D}_{\tilde{v}\tilde{w}} & \mathcal{D}_{\tilde{v}d} \\ 0 & I_{n_{\tilde{w}}} & 0 \end{bmatrix} \leq -\epsilon I. \tag{C23}$$

This DLMI can also be written in more compact notation using the state matrices of N_{scl}. Multiply inequality (C23) left and right by $[x^\top, \tilde{w}^\top, d^\top]$ and its transpose to show that $\tilde{V}(x(t), t) = x(t)^\top\tilde{P}(t)x(t)$ satisfies the following dissipation inequality:

$$\dot{\tilde{V}} + e_I^\top e_I - \gamma^2 d^\top d + \tilde{v}^\top\tilde{v} - \tilde{w}^\top\tilde{w} \leq -\epsilon\ d^\top d. \tag{C24}$$

Define $\tilde{d} := \gamma\ d$, $\tilde{\epsilon} := \epsilon\ \gamma^{-2}$ and combine the inputs $\tilde{w}$, $\tilde{d}$ together to rewrite the inequality (C24) as follows:

$$\dot{\tilde{V}} + \begin{bmatrix} \tilde{v} \\ e_I \end{bmatrix}^{\top} \begin{bmatrix} \tilde{v} \\ e_I \end{bmatrix} - \begin{bmatrix} \tilde{w} \\ \tilde{d} \end{bmatrix}^{\top} \begin{bmatrix} \tilde{w} \\ \tilde{d} \end{bmatrix} \leq -\tilde{\epsilon}\ \tilde{d}^{\top}\tilde{d}. \tag{C25}$$

Integrate over $[0, T]$ to obtain the following dissipation inequality:

$$\tilde{V}(x(T), T) - \tilde{V}(x(0), 0) + \left\| \begin{bmatrix} \tilde{v} \\ e_I \end{bmatrix} \right\|_{2,[0,T]}^2 - \left\| \begin{bmatrix} \tilde{w} \\ \tilde{d} \end{bmatrix} \right\|_{2,[0,T]}^2 \leq -\tilde{\epsilon}\|\tilde{d}\|_{2,[0,T]}^2. \tag{C26}$$

Note that $\tilde{V}(x(0), 0) = 0$ as $x(0) = 0$ and $\tilde{V}(x(T), T) = x(T)^{\top}\tilde{P}(T)x(T)$ with boundary condition $\tilde{P}(T) \geq F$ as shown earlier. Apply this boundary condition in inequality (C26) with the definition of F from Equation (14) to conclude:

$$\|e_E(T)\|_2^2 + \left\| \begin{bmatrix} \tilde{v} \\ e_I \end{bmatrix} \right\|_{2,[0,T]}^2 \leq \left\| \begin{bmatrix} \tilde{w} \\ \tilde{d} \end{bmatrix} \right\|_{2,[0,T]}^2 - \tilde{\epsilon}\|\tilde{d}\|_{2,[0,T]}^2. \tag{C27}$$

Divide both sides by $\left\| \begin{bmatrix} \tilde{w} \\ \tilde{d} \end{bmatrix} \right\|_{2,[0,T]}^2 < \infty$ and define $\hat{\epsilon} := \tilde{\epsilon}\|\tilde{d}\|_{2,[0,T]}^2 / \left\| \begin{bmatrix} \tilde{w} \\ \tilde{d} \end{bmatrix} \right\|_{2,[0,T]}^2$ to show that $\|N_{\text{scl}}\|_{[0,T]} \leq 1 - \hat{\epsilon}$. This proof can be worked backwards to prove **(2 ⇒ 1)**. ∎

Remark 1. If the IQC decision variables M and the state-space matrices of Ψ are constant on the given time horizon, then for sufficiently large horizon T, the RDE solution for the finite horizon factorization converges to that of the steady-state Algebric Riccati Equation (ARE). As a result, the state-space realization of the finite horizon factorization converges to that of an infinite horizon LTI spectral factorization. However, the ARE solution X for infinite horizon spectral factorization is sign indefinite, thus it fails to satisfy the terminal boundary condition on $\tilde{P}$. Thus, it is important to note in the above proof that in order to satisfy the boundary condition on storage function, one must use finite horizon factorization.